Assembly of Si-Substituted Heteropolyoxotantalate Architectures

Hanhan Chen, Haojie Xu, Xinyi Ma, Pengtao Ma, Jingping Wang,* and Jingyang Niu*

Henan Key Laboratory of Polyoxometalate Chemistry, College of Chemistry and Molecular Sciences, Henan University, Kaifeng, Henan 475004, P. R. China

Fax: +86-371-23886876; E-mail for Jingping Wang: jpwang@henu.edu.cn. and E-mail for Jingyang Niu: jyniu@henu.edu.cn.

Supporting Information

Experimental

Fig. S13. Fitted data of **1** under different temperatures at 95% RH. (a): 25°C; (b): 35°C, (c): 45°C; (d): 55°C; (e):65°C, and (f): 75°C.
Fig. S14. Nyquist plots for **1** under different temperatures at 75% RH. The solid lines are the best fits.
Fig. S15. Nyquist plots for **1** under different temperatures at 80% RH. The solid lines are the best fits.
Fig. S16. Nyquist plots for **1** under different temperatures at 85% RH. The solid lines are the best fits.
Fig. S17. Nyquist plots for **1** under different temperatures at 90% RH. The solid lines are the best fits.
Fig. S18. PXRD of **1** calculated (black), crystalline sample (red), and after the proton-conductive measurement (blue).
Fig. S19. Void analysis of **1**.
Fig. S20. In situ IR spectra of **1** under different water vapor pressure.
Fig. S21. Schematic diagram of hydrogen bonding networks consisting of water molecules inside the pore channels.
Fig. S22. IR spectrum of **1**.
Fig. S23. TG curve of **1**.

Experimental

Materials and Methods. All other chemicals were commercially purchased and utilized without undergoing additional purification. The potassium salt of the $K_8[Ta_6O_{19}]\cdot 17H_2O$ and $Na_{10}[A\text{-}\alpha\text{-}SiW_9O_{34}]\cdot 18H_2O$ precursor was synthesized according to the procedures outlined in the existing literature and its identity was verified through IR spectroscopy.[1,2] IR spectra of all compounds were obtained using a Bruker VERTEX 70 IR spectrometer with KBr pellets in the range of 4000–500 cm^{-1}. Thermogravimetric analysis (TGA) analyses was conducted using a NETZSCH STA 449 *F*5 Jupiter thermal analyzer under a flowing N_2 atmosphere with a heating rate of 10 °C min^{-1}. Powder X-ray diffraction (PXRD) data were conducted using an X-ray powder diffractometer (Bruker, *D*8 Advance) using Cu *K*α radiation (λ = 1.5418 Å) collected with the angular range (2θ) from 5° to 45° at room temperature. ICP analyses were achieved on a PerkinElmer Optima 2000 ICP-OES spectrometer. The proton conduction data was collected by impedance phase gain analyzers Solartron 1296.

Syntheses of $Li_7KNa_{11}H_6[Si_2Ta_{24}(O_2)_{20}O_{52}(OH)_9]\cdot 85H_2O$ (1). $K_8[Ta_6O_{19}]\cdot 17H_2O$ (2.805 g, 1.397mmol) was dissolved in 150 mL of H_2O. Subsequently, 30 mL 30% H_2O_2 solution was added. This was followed by the sequential addition of 7 mL 1M HCl and 3.345 g $Na_{10}[A\text{-}\alpha\text{-}SiW_9O_{34}]\cdot 18H_2O$. The suspension was agitated until a yellow clear solution was achieved, and 10 mL 6 M LiCl solution was added finally. The resulting solution was maintained at a temperature of 90 °C in a water bath for 3 h, followed by cooling to room temperature and subsequent filtration. Slow evaporation at room temperature led to the formation of colorless lamellar crystals for compound **1** after approximately one week. (yield: 8.60 % based on $K_8[Ta_6O_{19}]\cdot 17H_2O$). IR (KBr pellets, cm^{-1}): 3402 (br), 1643 (s), 951 (s), 891 (s), 844 (s), 741 (w), 515 (s).

X-ray crystallographic. The appropriate single crystal of compound **1** was affixed to the loop for

data collection at 150 K. Indexing and data collection was performed on a Bruker *D*8 VENTURE PHOTON II diffractometer, employing Mo *K*α radiation (λ = 0.71073 Å). Direct methods successfully located the tungsten atoms, and the remaining atoms were revealed through successive Fourier syntheses. Refinements were conducted through full-matrix least-squares on F^2 utilizing the SHELXL-2018 software suite for all the data.[3] In the final refinement, all the non-hydrogen atoms except those water O atoms were refined anisotropically. Most lattice water molecules were located by using a Fourier map, and the remaining lattice water molecules were determined by TGA results. All hydrogen atoms on water molecules could not be well located from the electron density map, which were directly included in the molecular formula.

Proton conduction experiments. AC impedance measurements were carried out Solartron Analytical ModuLab 1296 at frequencies ranging from 1 Hz to 10 MHz. The relative humidity was monitored with a STIK Corp CIHI-150BS3 incubator. The samples were pressed into a cylindrical compact of crystalline powder sample (~1 mm thickness × 3 mm diameter). Two silver electrodes were fastened to both edges of the pellet, forming four end terminals (quasi-four-probe method). Each humidity equilibrium and the thermal equilibrium were preserved for 1 h. The ZsimpWin software was utilized to model the equivalent circuit of the impedance data. The proton conductivity (σ) and activation energy (Ea) were calculated by the following two following equations:

$\sigma = d/RS$ (1)

$\sigma T = \sigma_0 \exp(-Ea/k_B T)$ (2)

where d is the thickness (cm) of the slice, S is the electrode area (cm^2), R is the resistance (Ω), σ_0 is the pre-exponential factor, T represents the absolute temperature, and k_B is the Boltzmann constant ($k_B = 8.63 \times 10^{-5}$ eV/K).

Table S1. Summary of heteropolyoxoniobate.

	Year	Compounds	Ref.
1	2002	$K_{12}[Ti_2O_2][SiNb_{12}O_{40}]\cdot 16H_2O$	4
2		$Na_{14}[H_2Si_4Nb_{16}O_{56}]\cdot 45.5H_2O$	
3	2004	$Na_{16}[SiNb_{12}O_{40}]\cdot 4H_2O$	5
4		$Na_{16}[GeNb_{12}O_{40}]\cdot 4H_2O$	
5	2005	$Na_{12}[Ti_2O_2][SiNb_{12}O_{40}]\cdot xH_2O$	6
6		$Na_{12}[Ti_2O_2][GeNb_{12}O_{40}]\cdot xH_2O$	
7		$Na_{10}[Nb_2O_2][SiNb_{12}O_{40}]\cdot xH_2O$	
8		$Na_{10}[Nb_2O_2][GeNb_{12}O_{40}]\cdot xH_2O$	
9	2006	$Na_{15}[(PO_2)_3PNb_9O_{34}]\cdot 22H_2O$	7
10	2007	$Li_{13}K[SiNb_{12}(OH)_2O_{38}]\cdot 17H_2O$	8
11	2007	$K_{10}[Nb_2O_2][GeNb_{12}O_{40}]\cdot 11H_2O$	9
12	2011	$K_{10}[Nb_2O_2(H_2O)_2][SiNb_{12}O_{40}]\cdot 12H_2O$	10
13	2011	$Cs_{13}Na[SiNb_{18}O_{54}]\cdot 22H_2O$	11
14		$Rb_{12}Na_2[SiNb_{18}O_{54}]\cdot 25H_2O$	
15		$K_{10}Na_2[H_2SiNb_{18}O_{54}]\cdot 33H_2O$	

16	2011	$[Cu(en)_2]_{3.5}[Cu(en)_2(H_2O)]\{[VNb_{12}O_{40}(VO)_2][Cu(en)_2]\}\cdot 17H_2O$	12
17	2012	$\{[Cu_6L_6(H_2O)_3][Nb_{10}V_4O_{40}(OH)_2]\}_2\cdot 13H_2O$	13
18	2012	$K_{14}Na[GaNb_{18}O_{54}]\cdot 28H_2O$	14
19		$K_{14}H[AlNb_{18}O_{54}]\cdot 31H_2O$	
20		$Rb_{15}[GaNb_{18}O_{54}]\cdot 35H_2O$	
21		$Cs_{13}Na_2[GaNb_{18}O_{54}]\cdot 20H_2O$	
22	2012	$[Cu(en)_2]_3\{[Cu(en)_2][H_2V_4Nb_6O_{30}]\}\cdot 12H_2O$	15
23		$[Cu(1,2\text{-dap})_2]_4[H_2V_4Nb_6O_{30}]\cdot 16H_2O$	
24		$[Cu(1,2\text{-dap})_2][Na_2(H_2O)_9][H_6V_4Nb_6O_{30}]\cdot 15H_2O$	
25	2012	$[Cu(en)_2]_3\{[Cu(en)_2][H_6SiNb_{18}O_{54}]\}\cdot 22H_2O$	16
26	2013	$TMA_9[PV_2Nb_{12}O_{42}]\cdot 19H_2O$	17
27	2013	$Na_4[Cu(en)_2(H_2O)_2]_5[Na_6Ge_8Nb_{32}O_{108}H_8(OH)_4]\cdot 41H_2O$	18
28	2013	$(C_2N_2H_{10})_6[(GeOH)_2Ge_2Nb_{16}H_2O_{54}]\cdot 25H_2O$	19
29		$[Cu(en)_2(H_2O)_2]_5K_{10}[K(GeOH)_2Ge_2Nb_{16}H_3O_{54}]_2\cdot 38H_2O$	
30	2013	$(TMA)_9[V_3Nb_{12}O_{42}]\cdot 18H_2O$	20
31	2013	$Rb_{13}[GeNb_{13}O_{41}]\cdot 23H_2O$	21
32		$Cs_{10.6}[H_{2.4}GeNb_{13}O_{41}]\cdot 27H_2O$	
33		$Cs_{18}H_6[(NbOH)SiNb_{12}O_{40}]_2\cdot 38H_2O$	
34	2014	$TMA_5[H_2TeNb_5O_{19}]\cdot 20H_2O$	22
35	2014	$[Cu(en)_2]_4[PNb_{12}O_{40}(VO)_6]\cdot(OH)_5\cdot 8H_2O$	23
36		$[Cu(enMe)_2]_4[PNb_{12}O_{40}(VO)_6]\cdot(OH)_5\cdot 6H_2O$	
37	2014	$\{Ni(en)_3\}_5H\{V^VNb_8V^{IV}{}_8O_{44}\}\cdot 9H_2O$	24
38		$(H_2en)Na_2[\{Zn(en)_2(Hen)\}\{Zn(en)_2(H_2O)\}_2\{PNb_8V^{IV}{}_8O_{44}\}]\cdot 11H_2O$	
39		$Na\{Cu(en)_2\}_3\{[Cu(en)_2]_2[PNb_8V^{IV}{}_8O_{44}]\}\cdot 11H_2O$	
40	2014	$\{Cu(en)_2\}_6\{GeNb_{12}V^{IV}{}_2O_{42}\}\cdot 20H_2O$	25
41		$\{Cu(en)_2\}_3K_2Na_4\{GeNb_{12}V^{IV}{}_2O_{42}\}\cdot 23H_2O$	
42		$\{Cu(en)_2\}_6\{SiNb_{12}V^{IV}{}_2O_{42}\}\cdot 18H_2O$	
43		$\{Cu(en)_2\}_3K_2Na_4\{SiNb_{12}V^{IV}{}_2O_{42}\}\cdot 19H_2O$	
44	2015	$TMA_9[PSb_2Nb_{12}O_{40}]\cdot 28H_2O$	26
45		$TMA_9[PNb_{14}O_{42}]\cdot 26H_2O$	
46		$TMA_{10}[H_5PNb_{12}O_{40}]\cdot 30.5H_2O$	
47	2015	$(TMA)_9H_3Nb_9P_5O_{41}\cdot 28H_2O$	27
48	2015	$[Cu(en)_2(H_2O)][Cu(en)_2]_4\{AsNb_9V_7O_{44}\}\cdot 8H_2O$	28
49		$[Cu(en)_2(H_2O)][Cu(en)_2]_4H\{AsNb_8V_8O_{44}\}\cdot 11H_2O$	
50		$\{V^V(H_2O)_6\}_{0.5}\{Co^{II}(en)_2\}_4\{SNb_8V^{IV}{}_8V^V{}_{1.25}O_{45.25}\}(OH)_{4.25}\cdot$	

		$3H_2O$	
51	2016	$[Co\text{-}(pn)_2]_4[HPNb_{10}V^{IV}{}_2O_{40}(V^{IV}O)_4]\cdot 17H_2O$	29
52		$[Co\text{-}(pn)_2]_4[HPNb_{10}V^{IV}{}_2O_{40}(V^{IV}O)_4]\cdot 17H_2O$	
53	2016	$Na_9H_4[VNb_{12}O_{40}\{NbO(CO_3)\}_2]\cdot 37H_2O$	30
54		$[Nb_{24}O_{76}V_4]^{12-}$	
55		$[V_3Nb_{24}O_{76}]^{17-}$	
56	2016	$[Cu(dap)_2]_4[AsNb_{12}O_{40}(VO)_4](OH)\cdot 7H_2O$	31
57	2017	$H_{13}[(CH_3)_4N]_{12}[PNb_{12}O_{40}(V^{V}O)_2\cdot(V^{IV}{}_4O_{12})_2]\cdot 22H_2O$	32
58	2017	$Na_{28}K_{16}H_{10}[Li_8\subset Nb_{114}O_{316}]$	33
59		$Na_{17}K_{12}H_{12}[Li_3K\subset Nb_{81}O_{225}]$	
60		$H_4Na_6K_{22}Cs_4[H_4Nb_{52}O_{150}]$	
61		$Na_{11}H_{25}[Cu(H_2O)_4]\{[Cu(en)_2]_3(K\subset H_3Cu_3Nb_{78}O_{222})\}$	
62		$Na_4K_2H_{16}[Cu(en)_2]_{0.5}\{[Cu(en)_2]_{9.5}(K\subset H_3Cu_4(en)Nb_{78}O_{222})\}$	
63	2017	$Na_{14}K_7H_5\{As_4Cu_4[Cu(H_2O)]_{12}Nb_{28}O_{109}\}\cdot 37.5H_2O$	34
64	2017	$K_3Na_2H_9(H_2en)_2[Fe_3Nb_{25}O_{76}]\cdot 17H_2O$	35
65	2017	$[Cu^{II}(C_2N_2H_8)_2]_4[Cu^{II}(C_2N_2H_8)_2(H_2O)_2]_2[PNb_{12}O_{40}V^{V}V^{IV}O_2]\cdot(OH)_2\cdot 11H_2O$	36
66	2017	$K_4[\{Cu(en)_2(H_2O)\}_4\{Cu(en)_2\}(H_2Te_2Nb_{24}O_{72})]\cdot 8H_2O$	37
67	2017	$H[Cu(en)_2(H_2O)]_8[Cu(en)_2(H_2O)_2]_2\{K_4[Cu(en)_2]_2[Cu(en)_2(GeNb_{18}O_{54})]_2\}[Nb_3W_3O_{19}]\cdot 32H_2O$	38
68	2017	$[Cu(en)_2]_4[Cu(en)_2(H_2O)_2]_2[SiNb_{12}V_2O_{42}]\cdot 14H_2O$	39
69		$[Cu(en)_2]_2[Cu(en)_2(H_2O)]_4[SiNb_{12}V_2O_{42}]\cdot 4H_2O$	
70		$[Cu(en)_2(H_2O)_2]_4[Cu(en)_2(H_2O)]_2[SiNb_{12}V_2O_{42}]\cdot 11H_2O$	
71	2019	$K_6[H\{Cu(phen)\}_{12}(H_2O)_2(Te_5Nb_{15.5}Cu_{0.5}O_{57})_2]\cdot 48H_2O$	40
72		$\{[\{Cu(phen)\}_6(H_2O)]_2[Cu(en)_2]_3(HTe_{10}Nb_{31}CuO_{114})\}\cdot 52H_2O$	
73		$\{[Cu(en)_2][Cu(en)_2(H_2O)][Cu(1,10\text{-}phen)][Cu(1,10\text{-}phen)(H_2O)]Nb_6O_{19}\}$	
74	2020	$K_2Na_2H_{16}(H_2O)_4[Cu(en)_2]_2[Cu(en)_2(H_2O)]_4\{[Cu(en)_2]_6[SiNb_{18}O_{54}]_3\}\cdot 34H_2O$	41
75	2020	$K_3[Nb_2O_2][H_7SiNb_{12}O_{40}]\cdot 16H_2O$	42
76		$[Cu(en)_2]_9[(VNb_{12}V_{1.69}Nb_{0.31}O_{42}en_{0.31})_2]\cdot 20.69H_2O$	

77	2020	$[\{Cu(en)(H_2O)_4\}\{Cu(en)_2(H_2O)\}\{Cu(en)_2(H_2O)_2\}]_{1.5}[H_8SiTe_8Nb_{15}O_{64}]\cdot 6H_2O$	43
78	2020	$H_{16}K_{24}Na_{26}[Cu_3(en)_6][(\beta\text{-}H_4Nb_{52}O_{150})_2]\cdot 88H_2O$	44
79	2020	$K_6Na_{17}[H_3\{Co(H_2O)_3\}_2(P_4Nb_9O_{40})_2]\ 24H_2O$	45
80	2020	$(CN_3H_6)_8K_4\{[Cu(phen)]_5[Nb_6O_{19}][As_2Nb_6O_{22}]\}_2\cdot 24H_2O$	46
81	2021	$K_{20}Na_{19}[H_{18.5}\{Cu(en)_2\}_2(H_4Cu_2Nb_{72}O_{205})]_2\cdot 77H_2O$	47
82	2021	$H_4K(CN_3H_6)_2\{[Cu_4(2,2\text{-bipy})_4(H_2O)_2][TeNb_9V_2O_{37}]\}\cdot 29H_2O$	48
83		$H_{0.5}K_5Na_{2.5}\{[Cu(en)H_2O]_3[TeNb_9V_3O_{39}]\}\cdot 10H_2O$	
84		$K_3Na_5\{[Cu(1,3\text{-dap})H_2O]_3[TeNb_9V_3O_{39}]\}\cdot 11H_2O$	
85	2021	$H_4Na_8K_6[Sb_2Nb_{24}O_{72}]\cdot 30H_2O$	49
86	2021	$K_2H[Cu(phen)(H_2O)]_4[Cu(phen)]_2[(LiNb_8Te_4O_{40})]\cdot 34H_2O$	50
87	2021	$H_9KNa_2(H_2O)_{10}[Co(H_2O)_2(SiNb_{18}O_{54})]\cdot 15H_2O$	51
88	2021	$[Cu(en)_2]_2\{[Cu(en)_2]_2K_4Ba_2(H_2O)_{13}(SiNb_{18}O_{54})\}_2\cdot 3en\cdot 52H_2O$	52
89		$H_6[Cu(en)_2]_2\{[Cu(en)_2]_2NaBa_2(H_2O)_7(SiNb_{18}O_{54})\}2\cdot 3en\cdot 50H_2O$	
90	2022	$H_5[Cu(H_2O)(en)_2]_2[Cu(H_2O)_2(en)_2]\{[Cu(en)_2(H_2O)]_2Eu(H_2O)_3Te_6Nb_{18}O_{64}(OH)_4\}\cdot 7H_2O$	53

L=1,10-phenanthroline;[13] 1,2-dap=1,2-diaminopropane;[15] en=ethylenediamine;[18, 28, 33, 35, 37–43, 47, 52, 53] enMe = 1,2-diaminopropane;[23] pn = 1,2-diaminopropane;[29] dap = 1,2- diaminopropane;[31] 1,10-phen =1,10-phenanthroline hydrate;[40] phen = 1,10-phenanthroline;[46, 50] 2,2'-bipy = 2,2'-bipyridine;[48] 1,3-dap = 1,3-diaminopropane;[48]

Table S2. Summary of heteropolyoxotantalate and corresponding synthetic methods.

Year	Compounds	Synthetic method	Reagents and Precursor	Ref.
2016	$[Ti_2Ta_8O_{28}]^{8-}$	Hydrothermal (140°C for 16 h), postprocessing	hydrous tantalum oxide (83 % w/w), $TMAOH\cdot 5H_2O$, titanium isopropoxide	54
2016	$[Ti_{12}Ta_6O_{44}]^{10-}$	Hydrothermal (150°C for 16 h), postprocessing	hydrous tantalum oxide (83 % w/w), $TMAOH\cdot 5H_2O$, titanium isopropoxide	54
2017	$[P_4(TaO_2)_6O_{25}]^{12-}$	80 °C for 3 h	$K_8[Ta_6O_{19}]\cdot 17H_2O$, H_2O_2, H_3PO_4	55
2017	$[P_4(TaO_2)_6O_{24}]^{10-}$	80 °C for 3 h	$K_8[Ta_6O_{19}]\cdot 17H_2O$, H_2O_2,	55

			H_3PO_4	
2019	$[Ln(H_2O)_6\{H_4(TaO_2)_6As_4O_{24}\}]^{3-}$	90 °C for 3 h	$K_8[Ta_6O_{19}]\cdot 17H_2O$, H_2O_2, $NaAsO_2$, $Ln(NO_3)_3\cdot 6H_2O$	56
2020	$[Se_4(TaO_2)_6(OH)_4O_{17}]^{4-}$	60 °C for 3 h	$K_8[Ta_6O_{19}]\cdot 17H_2O$, H_2O_2, Na_2SeO_3	57
2020	$[Ln(H_2O)_6(TaO_2)_6Se_4(OH)_3O_{18}]^{2-}$	stirring	$K_8[Ta_6O_{19}]\cdot 17H_2O$, H_2O_2, Na_2SeO_3, $LnCl_3\cdot 6H_2O$, CsCl	57
2022	$[Ni_2(H_2O)_{10}\{P_4Ta_6(O_2)_6O_{24}\}]^{6-}$	90 °C for 1 h	$K_8[Ta_6O_{19}]\cdot 17H_2O$, H_2O_2, $NiCl_2\cdot 6H_2O$, H_3PO_4, CsCl	58
2022	$[Zn(H_2O)_4\{P_4Ta_6(O_2)_6O_{24}\}]^{8-}$	90 °C for 1 h	$K_8[Ta_6O_{19}]\cdot 17H_2O$, H_2O_2, $ZnSO_4\cdot 7H_2O$, H_3PO_4, CsCl	58
2022	$[Cd(H_2O)_4\{P_4Ta_6(O_2)_6O_{24}\}]^{8-}$	90 °C for 1 h	$K_8[Ta_6O_{19}]\cdot 17H_2O$, H_2O_2, $CdCl_2$, H_3PO_4, CsCl	58
2023	$[Cu(en)_2(H_2O)_2]_2[Cu(en)_2][P_2O_7Ta_5O_{14}]^{-}$	80 °C for 3 d	$Na_8Ta_6O_{19}\cdot 24.5H_2O$, $Na_4P_2O_7\cdot 10H_2O$, en, $CuCl_2\cdot 2H_2O$	59
2023	$[Cu(en)_2(H_2O)_2][Cu(en)_2(H_2O)]\{[Cu\text{-}en)_2]_{1.5}[(P_2O_7)Ta_5O_{14}]\}$	80 °C for 3 d	$Na_8Ta_6O_{19}\cdot 24.5H_2O$, $Na_4P_2O_7\cdot 10H_2O$, en, $CuCl_2\cdot 2H_2O$	59
2023	$[Cu(en)_2]\{[Cu\text{-}en)_2]_2[(P_2O_7)Ta_5O_{14}]\}$	80 °C for 3 d	$Na_8Ta_6O_{19}\cdot 24.5H_2O$, $Na_4P_2O_7\cdot 10H_2O$, Na_2TeO_3, en, $CuCl_2\cdot 2H_2O$	59

en=ethylenediamine[59]

Table S3. Crystallographic data and structure refinements for **1**.

	1
Empirical formula	$KNa_{11}O_{158.5}Si_2Ta_{24}$
Formula weight	7226.97
Temperature / K	150
Crystal system	triclinic
Space group	*P*-1
a [Å]	19.495(5)
b [Å]	19.844(6)
c [Å]	21.896(7)
α [°]	73.755(10)
β [°]	81.216(7)
γ [°]	66.588(8)

V [Å^3]	7455(4)
Z	2
ρ_{calcd} [g cm^{-3}]	3.219
μ [mm^{-1}]	17.730
F(000)	6376.0
Index ranges	$-23 \leq h \leq 23$ $-23 \leq k \leq 23$ $-26 \leq l \leq 26$
Reflections collected	155083
Independent reflections	26519 [R_{int} = 0.0828]
data/restraints/ parameters	26519/60/1736
Goodness-of-fit on F^2	1.019
R_1, wR_2 [$I > 2\sigma(I)$]	0.0437, 0.1111
R_1, wR_2 [all data]	0.0560, 0.1222
Largest diff. Peak/hole/e Å^{-3}	4.05/-3.02

Table S4. Selected bond lengths (Å) of **1**.

Bond	Length	Bond	Length	Bond	Length
Ta16-O100	2.013(12)	Ta16-O36	1.988(11)	Ta7-O70	2.010(11)
Ta1-O101	2.026(13)	Ta20-O36	1.935(11)	Ta9-O70	2.002(11)
Ta21-O102	2.129(12)	Ta12-O37	2.102(11)	Ta17-O71	1.985(12)
Ta23-O102	2.172(12)	Ta15-O37	2.201(11)	Ta19-O72	2.000(13)
Ta3-O103	2.062(12)	Ta19-O38	1.917(11)	Ta23-O73	1.984(12)
Ta21-O104	2.017(11)	Ta20-O38	2.013(11)	Ta24-O73	1.983(11)
Ta22-O104	1.937(12)	Ta21-O39	2.168(11)	Ta13-O75	1.982(11)
Ta24-O105	1.989(13)	Ta22-O39	2.155(11)	Ta8-O76	2.135(11)
Ta1-O106	1.931(12)	Ta23-O39	2.159(11)	Ta9-O76	2.195(11)
Ta2-O106	2.023(12)	Ta24-O39	2.189(11)	Ta11-O78	1.997(12)
Ta4-O107	1.986(14)	Ta11-O40	1.996(11)	Ta2-O79	2.100(11)
Ta7-O110	1.984(12)	Ta13-O40	1.990(11)	Ta3-O79	2.155(12)
Ta23-O111	1.992(12)	Ta10-O41	1.962(11)	Ta23-O80	2.065(11)
Ta4-O113	1.996(13)	Ta11-O41	1.945(11)	Ta2-O82	2.009(12)
Ta6-O114	1.982(12)	Ta10-O42	2.045(11)	Ta4-O82	1.943(12)
Ta22-O116	1.995(13)	Ta12-O42	1.908(11)	Ta17-O83	1.940(12)
Ta3-O118	1.999(13)	Ta6-O43	2.008(11)	Ta19-O83	1.996(12)
Ta1-O120	1.990(12)	Ta10-O43	1.906(11)	Ta14-O84	1.997(12)
Ta3-O120	1.979(12)	Ta16-O44	1.997(11)	Ta4-O85	1.997(12)
Ta11-O122	1.973(12)	Ta2-O45	1.893(11)	Ta18-O86	2.005(12)

Ta7-O123	1.998(13)	Ta5-O45	2.021(11)	Ta1-O88	2.113(12)
Ta18-O126	2.004(12)	Ta4-O46	1.962(11)	Ta4-O88	2.153(12)
Ta8-O128	1.985(13)	Ta5-O46	1.944(11)	Ta1-O89	2.179(12)
Ta6-O132	2.005(13)	Ta17-O47	1.989(11)	Ta2-O89	2.187(12)
Ta8-O133	1.998(14)	Ta18-O47	1.971(11)	Ta3-O89	2.139(11)
Ta3-O134	1.981(12)	Ta14-O48	1.942(11)	Ta4-O89	2.161(11)
Ta2-O135	1.993(15)	Ta15-O48	1.947(11)	Ta24-O90	2.052(12)
Ta9-O136	2.004(12)	Ta20-O49	2.010(11)	Ta24-O91	1.983(14)
Ta2-O137	1.977(13)	Ta23-O49	1.916(11)	Ta22-O93	2.156(12)
Ta21-O140	1.986(15)	Ta16-O50	1.973(11)	Ta24-O93	2.116(12)
Ta22-O141	1.991(13)	Ta19-O50	2.013(11)	Ta19-O94	1.982(12)
Ta1-O146	1.971(13)	Ta13-O51	1.988(11)	Ta23-O95	1.991(12)
Ta11-O15	2.204(11)	Ta18-O52	2.123(12)	Ta9-O96	2.005(12)
Ta12-O15	2.124(11)	Ta19-O52	2.132(12)	Ta12-O97	1.973(13)
Ta13-O15	2.172(11)	Ta8-O53	1.925(11)	Ta21-O98	2.043(12)
Ta14-O15	2.172(11)	Ta10-O53	1.972(11)	Ta24-O98	1.918(12)
Ta1-O152	1.962(14)	Ta6-O54	2.176(11)	Si1-O101	1.622(13)
Ta21-O155	1.986(14)	Ta7-O54	2.117(11)	Si1-O103	1.631(12)
Ta5-O16	1.926(11)	Ta15-O55	1.907(11)	Si1-O108	1.627(13)
Ta9-O16	2.006(11)	Ta18-O55	2.015(12)	Si1-O85	1.648(12)
Ta16-O18	2.158(10)	Ta5-O56	1.992(12)	Si2-O90	1.624(13)
Ta17-O18	2.198(10)	Ta6-O56	1.921(12)	Si2-O69	1.641(12)
Ta18-O18	2.154(10)	Ta20-O57	2.036(12)	Si2-O80	1.638(11)
Ta19-O18	2.189(11)	Ta21-O57	1.886(12)	Si2-O108	1.617(13)
Ta15-O20	1.987(11)	Ta20-O58	1.942(11)	O44-O100	1.513(16)
Ta16-O20	1.923(11)	Ta22-O58	1.979(11)	O51-O75	1.502(16)
Ta13-O22	2.154(10)	Ta16-O59	2.168(11)	O60-O71	1.514(17)
Ta14-O22	2.133(10)	Ta17-O59	2.138(11)	O63-O84	1.531(16)
Ta9-O24	1.901(11)	Ta17-O60	1.966(12)	O68-O97	1.526(17)
Ta10-O24	2.021(11)	Ta6-O61	1.982(11)	O72-O94	1.496(17)
Ta5-O26	1.987(11)	Ta8-O61	1.974(11)	O78-O122	1.503(17)
Ta7-O26	1.929(11)	Ta7-O62	1.987(12)	O86-O126	1.534(17)
Ta15-O28	1.954(10)	Ta8-O62	1.994(11)	O91-O105	1.534(19)
Ta17-O28	1.965(10)	Ta14-O63	1.999(12)	O95-O111	1.510(17)
Ta10-O29	1.962(11)	Ta3-O64	1.922(11)	O96-O136	1.501(16)
Ta13-O29	1.987(11)	Ta5-O64	2.003(11)	O107-O113	1.529(19)
Ta13-O31	1.947(10)	Ta12-O65	1.983(11)	O110-O123	1.497(17)
Ta15-O31	1.990(10)	Ta14-O65	1.996(11)	O114-O132	1.508(17)
Ta6-O33	2.155(11)	Ta11-O66	2.088(11)	O116-O141	1.510(18)
Ta7-O33	2.181(11)	Ta12-O66	2.113(11)	O118-O134	1.535(18)
Ta8-O33	2.186(11)	Ta11-O67	2.002(12)	O128-O133	1.546(18)
Ta9-O33	2.141(11)	Ta14-O67	1.972(12)	O135-O137	1.498(19)
Ta18-O35	1.929(11)	Ta12-O68	1.990(12)	O140-O155	1.52(2)

Ta20-O35	1.974(11)	Ta22-O69	2.005(11)	O146-O152	1.508(19)

Table S5. Summary of polyperoxo-polyoxometalate.

	Year	Compounds	Ref.
1	1997	$(H_3Cs_{5.6}K_{3.1}Li_{0.3})[P_2W_{12}(NbO_2)_6O_{56}]\cdot 11H_2O$	60
2	2010	$Cs_{6.5}K_{0.5}[GeW_9(NbO_2)_3O_{37}]\cdot 6H_2O$	61
3	2011	$Cs_5K[AsW_9(NbO_2)_3O_{37}]\cdot 7H_2O$	62
4	2011	$K_{12}[Zr_2(O_2)_2(\alpha\text{-}SiW_{11}O_{39})_2]\cdot 25H_2O$	63
5		$K_{12}[Zr_2(O_2)_2(\alpha\text{-}GeW_{11}O_{39})_2]\cdot 25H_2O$	
6		$K_{10.5}Rb_{1.5}[Hf_2(O_2)_2(\alpha\text{-}SiW_{11}O_{39})_2]\cdot 21H_2O$	
7		$K_{18}[Zr_6(O_2)_6(OH)_6(\gamma\text{-}SiW_{10}O_{36})_3]\cdot 59H_2O$	
8		$K_{18}[Hf_6(O_2)_6(OH)_6(\gamma\text{-}SiW_{10}O_{36})_3]\cdot 59H_2O$	
9	2012	$Na_6Li_{24}\{[W_5O_{21}]_3[(U^{VI}O_2)_2(\mu\text{-}O_2)]_3\}$	64
10	2012	$K_5Na_4[P_2W_{15}O_{59}(TaO_2)_3]\cdot 17H_2O$	65
11		$Cs_3K_{3.5}H_{0.5}[SiW_9(TaO_2)_3O_{37}]\cdot 9H_2O$	
12	2014	$K_4Na_4[H_6P_2W_{12}Nb_4O_{59}(NbO_2)_2]_2\cdot 48H_2O$	66
13	2017	$Cs_3[H_9P_4Ta_6(O_2)_6O_{25}]\cdot 9H_2O$	55
14		$(CN_3H_6)_6[H_4P_4Ta_6(O_2)_6O_{24}]\cdot 4H_2O$	
15	2019	$Cs_3[Ln\text{-}(H_2O)_6\{H_4(TaO_2)_6As_4O_{24}\}]\cdot 7H_2O$	56
16	2019	$Na_{24}[Ce^{IV}_6(O_2)_9(GeW_{10}O_{37})_3]\cdot 100H_2O$	67
17		$Na_{24}[Ce_6(O_2)_9(SiW_{10}O_{37})_3]\cdot\sim 100H_2O$	
18	2020	$Cs_2KH[(TaO_2)_6Se_4(OH)_4O_{17}]\cdot 10H_2O$	57
19		$CsK[Ln(H_2O)_6(TaO_2)_6Se_4(OH)_3O_{18}]\cdot 11H_2O$	
20	2020	$Cs_3H_3[Ni_2(H_2O)_4\{P_4Ta_6(O_2)_6O_{24}\}]\cdot 7H_2O$	58
21		$Cs_3NaH_4[Zn(H_2O)_4\{P_4Ta_6(O_2)_6O_{24}\}]\cdot 13H_2O$	
22		$Cs_3NaH_4[Cd(H_2O)_4\{P_4Ta_6(O_2)_6O_{24}\}]\cdot 8H_2O$	
23	2022	$CsK[Ln(H_2O)_6Se_4(TaO_2)_6(OH)_3O_{18}]\cdot nH_2O$	68

Table S6. Bond angles (°) for Op−Ta−Op in **1**.

Bond	Angle	Bond	Angle
O146-Ta1-O152	45.1(6)	O51-Ta13-O75	44.5(5)
O135-Ta2-O137	44.3(5)	O63-Ta14-O84	45.0(5)
O118-Ta3-O134	45.4(5)	O44-Ta16-O100	44.3(5)
O107-Ta4-O113	45.1(5)	O60-Ta17-O71	45.1(5)
O114-Ta6-O132	44.4(5)	O86-Ta18-O126	45.0(5)
O110-Ta7-O123	44.2(5)	O72-Ta19-O94	44.2(5)
O128-Ta8-O133	45.7(5)	O140-Ta21-O155	44.9(6)

O96-Ta9-O136	44.0(5)	O116-Ta22-O141	44.5(5)
O78-Ta11-O122	44.5(5)	O95-Ta23-O111	44.5(5)
O68-Ta12-O97	45.3(5)	O91-Ta24-O105	45.4(5)

Table S7. Assignment of peaks of **1** in negative mode mass spectrum.

Species	Sim. m/z	Exp. m/z
$[KH_{27}Si_2Ta_{24}(O_2)_{20}O_{52}(OH)_9]^{6-}$	1013.40	1013.42
$[KLiH_{26}Si_2Ta_{24}(O_2)_{20}O_{52}(OH)_9]^{6-}$	1014.40	1014.43
$[KLi_2H_{25}Si_2Ta_{24}(O_2)_{20}O_{52}(OH)_9]^{6-}$	1015.40	1015.43
$[KNaH_{26}Si_2Ta_{24}(O_2)_{20}O_{52}(OH)_9]^{6-}$	1017.06	1017.09
$[KNaLiH_{25}Si_2Ta_{24}(O_2)_{20}O_{52}(OH)_9]^{6-}$	1018.06	1018.09
$[K_2H_{26}Si_2Ta_{24}(O_2)_{20}O_{52}(OH)_9]^{6-}$	1019.72	1019.75
$[K_2LiH_{25}Si_2Ta_{24}(O_2)_{20}O_{52}(OH)_9]^{6-}$	1020.72	1020.75
$[K_2Li_2H_{24}Si_2Ta_{24}(O_2)_{20}O_{52}(OH)_9]^{6-}$	1021.72	1021.76
$[K_2NaH_{25}Si_2Ta_{24}(O_2)_{20}O_{52}(OH)_9]^{6-}$	1023.38	1023.41
$[K_2NaLiH_{24}Si_2Ta_{24}(O_2)_{20}O_{52}(OH)_9]^{6-}$	1024.39	1024.42
$[K_3H_{25}Si_2Ta_{24}(O_2)_{20}O_{52}(OH)_9]^{6-}$	1026.05	1026.07
$[K_3LiH_{24}Si_2Ta_{24}(O_2)_{20}O_{52}(OH)_9]^{6-}$	1027.05	1027.07
$[K_3Li_2H_{23}Si_2Ta_{24}(O_2)_{20}O_{52}(OH)_9]^{6-}$	1028.05	1028.07
$[K_3NaH_{24}Si_2Ta_{24}(O_2)_{20}O_{52}(OH)_9]^{6-}$	1029.71	1029.74
$[K_3NaLiH_{23}Si_2Ta_{24}(O_2)_{20}O_{52}(OH)_9]^{6-}$	1030.71	1030.74
$[K_3NaLi_2H_{22}Si_2Ta_{24}(O_2)_{20}O_{52}(OH)_9]^{6-}$	1031.71	1031.74
$[K_3NaLi_3H_{21}Si_2Ta_{24}(O_2)_{20}O_{52}(OH)_9]^{6-}$	1032.71	1032.74
$[K_4LiH_{23}Si_2Ta_{24}(O_2)_{20}O_{52}(OH)_9]^{6-}$	1033.37	1033.40
$[K_4Li_2H_{22}Si_2Ta_{24}(O_2)_{20}O_{52}(OH)_9]^{6-}$	1034.38	1034.40
$[K_4Li_3H_{21}Si_2Ta_{24}(O_2)_{20}O_{52}(OH)_9]^{6-}$	1035.38	1035.40
$[K_4NaLiH_{22}Si_2Ta_{24}(O_2)_{20}O_{52}(OH)_9]^{6-}$	1037.04	1037.07
$[K_4NaLi_2H_{21}Si_2Ta_{24}(O_2)_{20}O_{52}(OH)_9]^{6-}$	1038.04	1038.06
$[K_4NaLi_3H_{20}Si_2Ta_{24}(O_2)_{20}O_{52}(OH)_9]^{6-}$	1039.04	1039.08
$[K_5LiH_{22}Si_2Ta_{24}(O_2)_{20}O_{52}(OH)_9]^{6-}$	1039.70	1039.73
$[K_5Li_2H_{21}Si_2Ta_{24}(O_2)_{20}O_{52}(OH)_9]^{6-}$	1040.70	1040.72
$[K_5Li_3H_{20}Si_2Ta_{24}(O_2)_{20}O_{52}(OH)_9]^{6-}$	1041.70	1041.73
$[K_5Li_4H_{19}Si_2Ta_{24}(O_2)_{20}O_{52}(OH)_9]^{6-}$	1042.70	1042.72
$[K_5NaLiH_{21}Si_2Ta_{24}(O_2)_{20}O_{52}(OH)_9]^{6-}$	1043.36	1043.39
$[K_5NaLi_2H_{20}Si_2Ta_{24}(O_2)_{20}O_{52}(OH)_9]^{6-}$	1044.37	1044.39
$[K_5NaLi_3H_{19}Si_2Ta_{24}(O_2)_{20}O_{52}(OH)_9]^{6-}$	1045.37	1045.39
$[K_6Li_2H_{20}Si_2Ta_{24}(O_2)_{20}O_{52}(OH)_9]^{6-}$	1047.03	1047.06
$[Na_2H_{27}Si_2Ta_{24}(O_2)_{20}O_{52}(OH)_9]^{5-}$	1217.48	1217.42
$[K_3Na_2Li_3H_{21}Si_2Ta_{24}(O_2)_{20}O_{52}(OH)_9]^{5-}$	1244.26	1244.18
$[K_3Na_2Li_4H_{20}Si_2Ta_{24}(O_2)_{20}O_{52}(OH)_9]^{5-}$	1245.46	1245.38
$[K_4NaLi_3H_{21}Si_2Ta_{24}(O_2)_{20}O_{52}(OH)_9]^{5-}$	1247.45	1247.37
$[K_4Na_2Li_4H_{19}Si_2Ta_{24}(O_2)_{20}O_{52}(OH)_9]^{5-}$	1253.05	1252.98
$[K_5Li_6H_{18}Si_2Ta_{24}(O_2)_{20}O_{52}(OH)_9]^{5-}$	1254.25	1254.18
$[K_5NaLi_4H_{19}Si_2Ta_{24}(O_2)_{20}O_{52}(OH)_9]^{5-}$	1256.24	1256.17

$[K_5Na_3H_{21}Si_2Ta_{24}(O_2)_{20}O_{52}(OH)_9]^{5-}$	1259.76	1259.83
$[K_5NaLi_2H_{22}Si_2Ta_{24}(O_2)_{20}O_{52}(OH)_9]^{4-}$	1567.05	1567.10
$[K_6Li_2H_{22}Si_2Ta_{24}(O_2)_{20}O_{52}(OH)_9]^{4-}$	1571.05	1571.10
$[K_5Na_2Li_3H_{20}Si_2Ta_{24}(O_2)_{20}O_{52}(OH)_9]^{4-}$	1574.55	1574.59
$[K_5Na_2Li_4H_{19}Si_2Ta_{24}(O_2)_{20}O_{52}(OH)_9]^{4-}$	1576.05	1576.10
$[K_5Na_2Li_6H_{17}Si_2Ta_{24}(O_2)_{20}O_{52}(OH)_9]^{4-}$	1579.06	1579.08
$[K_5Na_2Li_8H_{15}Si_2Ta_{24}(O_2)_{20}O_{52}(OH)_9]^{4-}$	1582.06	1582.08
$[K_5Na_3Li_6H_{16}Si_2Ta_{24}(O_2)_{20}O_{52}(OH)_9]^{4-}$	1584.59	1584.10
$[K_5Na_5LiH_{19}Si_2Ta_{24}(O_2)_{20}O_{52}(OH)_9]^{4-}$	1587.53	1587.56
$[K_5Na_5Li_2H_{18}Si_2Ta_{24}(O_2)_{20}O_{52}(OH)_9]^{4-}$	1589.03	1589.04

Table S8. Data of proton conductivity σ ($S\cdot cm^{-1}$) of **1** at various RH conditions under 25°C RH.

T (°C)	**1**
75	1.23×10^{-7}
80	1.44×10^{-5}
85	3.92×10^{-5}
90	6.54×10^{-5}
95	8.13×10^{-4}

Table S9. Data of proton conductivity σ ($S\cdot cm^{-1}$) of **1** at various temperature conditions under 95% RH.

T (°C)	**1**
25	8.13×10^{-4}
35	1.11×10^{-3}
45	1.67×10^{-3}
55	2.61×10^{-3}
65	3.21×10^{-3}
75	3.63×10^{-3}

Table S10. A comparison of the proton conductivity of **1** and all polyoxotantalates-based crystalline conducting materials.

POMs-based crystalline conducting materials	Proton conductivity ($S\ cm^{-1}$)	Relative Humidity	Temperature (°C)	*Ea* (eV)	Ref.
1	8.13×10^{-4}	95%	25	0.29	This work
	3.63×10^{-3}	95%	75		
$K_{12}Na_{14}H_{7.4}[Fe_{10.7}Ta_{1.3}O_8(OH)_8(H_2O)_2(Ta_6O_{19})_6]\cdot114.5H_2O$	9.24×10^{-4}	85%	25	0.50	69
	2.61×10^{-2}	85%	85		

$H[Co^{III}(en)_3]_3[Co^{III}(en)_2O](C_2O_4)\{(Ta_6O_{19})_2[Co^{II}(C_2O_4)(H_2O_2)]_2[Co^{III}(en)(H_2O)]_2\}\cdot 41H_2O$	4.67×10^{-6}	98%	25	0.68	70
	1.10×10^{-3}	98%	85		
$[Co^{III}(en)_3]_4C_2O_4\{Ta_6O_{19}[Co^{III}(en)]\}_2\cdot 66H_2O$	8.05×10^{-4}	98%	25	0.85	70
	5.76×10^{-2}	98%	85		
$H_2[Cu(en)_2(H_2O)_2]\{[Cu(en)_2]_4[Cu(en)(Ta_6O_{19})]_2\}14H_2O$	9.90×10^{-5}	98%	25	0.56	71
	1.04×10^{-2}	98%	75		
$[Ni_2(H_2O)_{10}\{P_4Ta_6(O_2)_6O_{24}\}]^{6-}$	3.69×10^{-5}	90%	25	0.39	58
	1.22×10^{-3}	90%	85		
$H_2[Co(en)_3]_3Ta_6O_{19}$	9.16×10^{-7}	98%	25	0.42/1.828	72
	2.67×10^{-3}	98%	85		
$Na_2(H_2O)_6H_2[Co(en)_3]_2Ta_6O_{19}$	6.32×10^{-7}	98%	25	0.66	72
	6.18×10^{-4}	98%	85		

Table S11. A comparison of the proton conductivity of **1** and some other recent representative POMs-based crystalline conducting materials.

POMs-based crystalline conducting materials	Proton conductivity (S cm^{-1})	Relative Humidity	Temperature (°C)	*Ea* (eV)	Ref.
1	8.13×10^{-4}	95%	25	0.29	This work
	3.63×10^{-3}	95%	95		
$H_6[Cu(en)_2]_8[Ge_{12}O_6(OH)_8Nb_{38}O_{120}]\cdot 34H_2O$	5.73×10^{-6}	98%	25	0.60	73
	3.04×10^{-4}	98%	85		
$H_8[Cu(en)_2]_7[Ge_{12}O_8(OH)_4Nb_{38}O_{120}]\cdot 28H_2O$	8.92×10^{-6}	98%	25	0.47	73
	1.62×10^{-4}	98%	85		
$Na_{16}H_{22}[(B\text{-}\beta\text{-}SbW_9O_{33})_6(W_3RuO_7)_2(W_4O_{11})]\cdot 118H_2O$	1.12×10^{-3}	55%	30	0.40	74
	5.41×10^{-3}	55%	60		
$Na_{5.5}H_{6.5}[(SbW_9O_{33})_2\{WO_2(OH)\}_2\{WO_2\}RuC_7H_3NO_4]\cdot 36H_2O$	4.90×10^{-3}	75%	25	0.31	75
	2.97×10^{-2}	75%	75		
$[Cu(en)_2(H_2O)]_2[Cu(en)_2]_{10}H_{97}[Dy_{10}Nb_{190}]^{7-}$	1.19×10^{-4}	98%	25	0.54	76
	3.75×10^{-3}	98%	85		
$[(AsW_9O_{33})_6\{W_2O_5(H_2O)(_{DL}\text{-}Ala)\}_2\{W_3O_6(H_2O)(_{DL}\text{-}Ala)\}_2\{W_2O_5(_{DL}\text{-}Ala)\}]$	2.83×10^{-4}	75%	65	0.54	77
$[As_4W_{48}O_{168}]^{36-}$	1.30×10^{-3}	98%	25	0.26	78
	5.00×10^{-3}	98%	75		
$[As_2W_{21}O_{77}(H_2O)_3]^{22-}$	8.20×10^{-5}	98%	25	0.39	78

	6.40×10^{-4}	98%	75		
$H_4[Cu(en)_2]_4\{K_4(H_2O)_2[Cu(en)_2]_5[Cu_5(trz)_2(en)_4(OH)_2][Dy_2Cu_2(en)_2(CO_3)_3(H_2O)_2(OH)_3][Dy(H_2O)_4][DyNb_{23}O_{68}(H_2O)_4]_2\}\ 60H_2O$	4.68×10^{-6}	98%	25	1.03	79
	3.42×10^{-3}	98%	85		
$H\{La_4(L)_2(H_2O)_{21}[Zr_3(OH)_3(PW_9O_{34})_2]\}\ 15H_2O$	6.94×10^{-4}	98%	35	0.24	80
	2.13×10^{-3}	98%	85		
$H\{Ce_4(L)_2(H_2O)_{21}[Zr_3(OH)_3(PW_9O_{34})_2]\}\ 15H_2O$	5.99×10^{-4}	98%	35	0.28	80
	2.35×10^{-3}	98%	85		
$H\{Pr_4(L)_2(H_2O)_{21}[Zr_3(OH)_3(PW_9O_{34})_2]\}\ 15H_2O$	1.78×10^{-3}	98%	35	0.30	80
	7.53×10^{-3}	98%	85		
$\{[Co(en)_2(SO_3)][Te_4Nb_{24}O_{79}]\}^{20-}$	8.13×10^{-5}	75%	25	0.28	81
	3.05×10^{-4}	75%	60		
$\{[Cu(en)_2]_{10}[Nb_{68}O_{182}(OH)_8(H_2O)_{10}]\}^{12-}$	9.67×10^{-5}	98%	25	0.53	82
	5.71×10^{-3}	98%	75		
$[Co(H_2O)_6]_2\{[Co(H_2O)_4]_4[WZn_3(H_2O)_2(ZnW_9O_{34})_2]\}$	7.61×10^{-6}	98%	25	0.24	83
	3.55×10^{-4}	98%	85		
$\{[P_2W_{15}Nb_3O_{62}]_2(4PBA)_2((4PBA)_2O)\}^{16-}$	7.78×10^{-2}	98%	90	0.66	84
$\{[W_{14}Ce^{IV}_6O_{61}]([W_3Bi_6Ce^{III}_3(H_2O)_3O_{14}][BiW_9O_{33}]_3)_2\}^{34-}$	2.40×10^{-3}	90%	25	0.68	85
$\{[Na(NO_3)(H_2O)]_4[Al_{16}(OH)_{24}(H_2O)_8(P_8W_{48}O_{184})]\}^{16-}$	9.10×10^{-3}	85%	25	0.32	86
	4.50×10^{-2}	85%	85		
$[Na_6(H_2O)_{12}]_4[K_{42}Ge_8W_{72}O_{272}(H_2O)_{60}]^{14-}$	3.30×10^{-3}	98%	30	0.52	87
	6.80×10^{-3}	98%	80		
$[La_{27}Ge_{10}W_{106}O_{406}(OH)_4(H_2O)_{24}]^{59-}$	4.00×10^{-5}	98%	30	0.42	88
	1.50×10^{-2}	98%	85		
$[Ce^{III}(H_2O)_6]\{[Ce^{IV}_7Ce^{III}_3O_6(OH)_6(CO_3)(H_2O)_{11}][(P_2W_{16}O_{59})]_3\}^{16-}$	1.95×10^{-7}	75%	30	0.36	89
	1.50×10^{-5}	75%	100		
$\{[Na(H_2O)_4]NaAs_2W_{22}(CH_3COO)_2O_{76}Rh_2(N(CH_3)_2)_2\}^{8-}$	6.43×10^{-5}	80%	25	0.36	90
	3.23×10^{-4}	80%	65		
$Cu_6(Trz)_{10}(H_2O)_4[H_2SiW_{12}O_{40}]\cdot 8H_2O$	5.40×10^{-8}	95%	45	0.34	91
	1.84×10^{-6}	95%	95		
$[La_3(H_2O)_{22}][P_2W_{15}Ta_3O_{62}]$	3.24×10^{-4}	98%	25	0.36	92
	1.26×10^{-2}	98%	95		
$[\{As^{III}_5O_4(OH)_3\}_2(P_8W_{48}O_{184})]^{32-}$	1.20×10^{-3}	70%	35	0.61	93
	1.20×10^{-2}	70%	85		

Table S12. Data of proton conductivity σ ($S \cdot cm^{-1}$) of **1** at various temperature conditions under 75% RH.

T (°C)	**1**
25	1.23×10^{-7}
35	5.63×10^{-7}
45	3.27×10^{-6}
55	1.40×10^{-5}
65	3.42×10^{-5}
75	8.31×10^{-5}
85	1.26×10^{-4}

Table S13. Data of proton conductivity σ ($S \cdot cm^{-1}$) of **1** at various temperature conditions under 80% RH.

T (°C)	**1**
25	1.44×10^{-5}
35	3.70×10^{-5}
45	5.43×10^{-5}
55	8.43×10^{-5}
65	1.23×10^{-4}
75	1.74×10^{-4}
85	2.40×10^{-4}

Table S14. Data of proton conductivity σ ($S \cdot cm^{-1}$) of **1** at various temperature conditions under 85% RH.

T (°C)	**1**
25	3.92×10^{-5}
35	8.68×10^{-5}
45	1.28×10^{-4}
55	1.83×10^{-4}
65	2.83×10^{-4}
75	3.80×10^{-4}
85	5.00×10^{-4}

Table S15. Data of proton conductivity σ ($S \cdot cm^{-1}$) of **1** at various temperature conditions under 90% RH.

T (°C)	**1**
25	6.54×10^{-5}
35	1.30×10^{-4}
45	2.03×10^{-4}
55	3.04×10^{-4}

65	3.86×10^{-4}
75	4.77×10^{-4}
85	6.36×10^{-4}

Table S16. Selected hydrogen bond distances for **1**.

D–H···A	d(D···A)(Å)	D–H···A	d(D···A)(Å)
O(6W)–H···O54	2.9380(154)	O(31W)–H···O52	2.8121(148)
O(7W)–H···O31	2.7607(123)	O(33W)–H···O98	2.7395(248)
O(10W)–H···O52	2.7517(120)	O(38W)–H···O96	2.7596(156)
O(11W)–H···O8	2.7763(145)	O(40W)–H···O33	2.7893(182)
O(13W)–H···O55	2.8085(156)	O(43W)–H···O39	2.6880(178)
O(17W)–H···O74	2.7688(128)	O(46W)–H···O42	2.7690(177)
O(19W)–H···O91	2.6195(136)	O(47W)–H···O49	2.6908(198)
O(23W)–H···O48	2.7421(161)	O(54W)–H···O56	2.7981(254)
O(26W)–H···O71	2.8674(206)	O(58W)–H···O48	2.8489(360)
O(30W)–H···O47	2.7390(135)		

Table S17. BVS values for Ta and Si atoms in **1**.

Atoms	BVS value	Atoms	BVS value	Atoms	BVS value
Ta1	5.43	Ta10	5.13	Ta19	5.32
Ta2	5.39	Ta11	5.35	Ta20	5.01
Ta3	5.26	Ta12	5.39	Ta21	5.32
Ta4	5.40	Ta13	5.28	Ta22	5.29
Ta5	5.11	Ta14	5.32	Ta23	5.22
Ta6	5.27	Ta15	5.03	Ta24	5.34
Ta7	5.33	Ta16	5.33	Si1	3.90
Ta8	5.32	Ta17	5.31	Si2	3.97
Ta9	5.30	Ta18	5.32		

Table S18. BVS values for O atoms in **1**.

Atoms	BVS value	Atoms	BVS value	Atoms	BVS value
O100	0.78	O20	1.83	O61	1.71
O101	1.76	O22	1.09	O62	1.65
O102	1.07	O24	1.81	O63	0.81
O103	1.66	O26	1.81	O64	1.79
O104	1.72	O28	1.80	O65	1.66
O105	0.83	O29	1.73	O66	1.23
O106	1.72	O31	1.76	O67	1.67
O107	0.84	O33	2.06	O68	0.83
O108	2.01	O35	1.84	O69	1.75

O110	0.84	O36	1.79	O70	1.59
O111	0.82	O37	1.08	O71	0.84
O113	0.81	O38	1.79	O72	0.81
O114	0.85	O39	2.05	O73	1.68
O116	0.82	O40	1.64	O75	0.85
O118	0.81	O41	1.83	O76	1.03
O120	1.68	O42	1.75	O78	0.81
O122	0.87	O43	1.83	O79	1.14
O123	0.81	O44	0.81	O80	1.64
O126	0.80	O45	1.84	O82	1.73
O128	0.84	O46	1.83	O83	1.76
O132	0.79	O47	1.70	O84	0.81
O133	0.81	O48	1.87	O85	1.75
O134	0.85	O49	1.79	O86	0.79
O135	0.82	O50	1.64	O88	1.12
O136	0.80	O51	0.83	O89	2.05
O137	0.86	O52	1.14	O90	1.70
O140	0.84	O53	1.86	O91	0.84
O141	0.83	O54	1.09	O93	1.11
O146	0.87	O55	1.81	O94	0.85
O15	2.05	O56	1.82	O95	0.83
O152	0.89	O57	1.83	O96	0.79
O155	0.84	O58	1.79	O97	0.87
O16	1.78	O59	1.07	O98	1.72
O18	2.01	O60	0.88		

Table S19. Calculated and found analyses of Na, K, Li, Si, and Ta with massic ratios in **1**.

	Na (%)	**K (%)**	**Li (%)**	**Si (%)**	**Ta (%)**
calcd	3.20	0.49	0.61	0.71	54.96
found	3.15	0.46	0.65	0.67	54.75

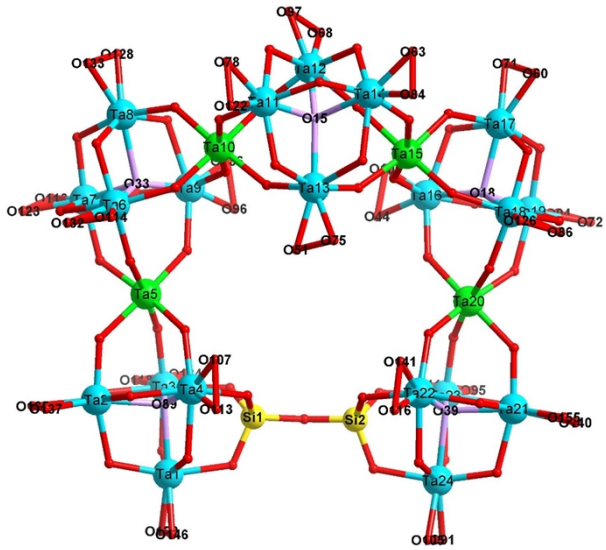

Fig. S1. The ball-and-stick representation of **1a**. Color code: sea blue and green spheres: Ta; lavender spheres: μ_4-O spheres; red spheres: O; yellow spheres: Si.

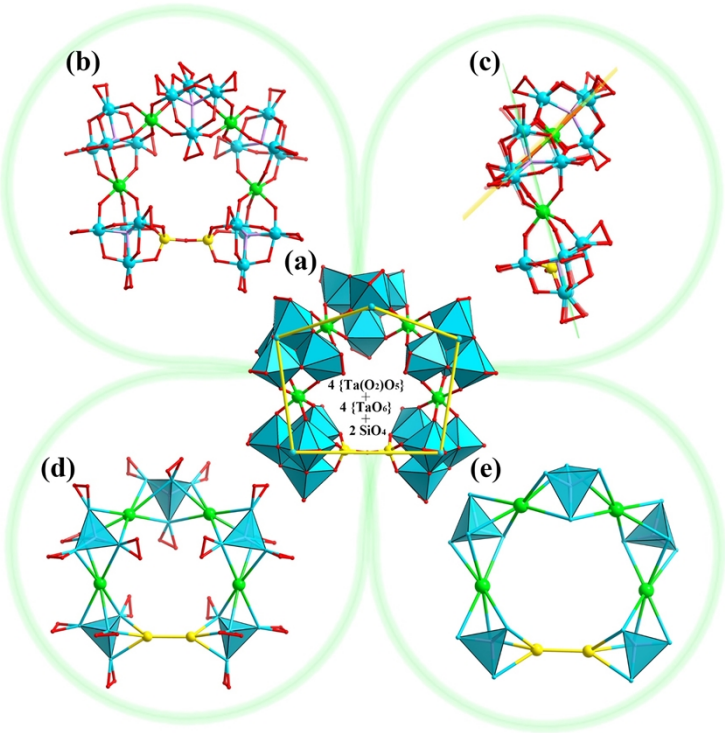

Fig. S2. (a) The polyhedral/ball-and-stick representation of **1a**. (b) The ball-and-stick representation of **1a**. (c) The side view of **1a**. (d and e) The simplified diagram of **1a**. (Si, yellow; Ta, sea blue and green; O, red and lavender).

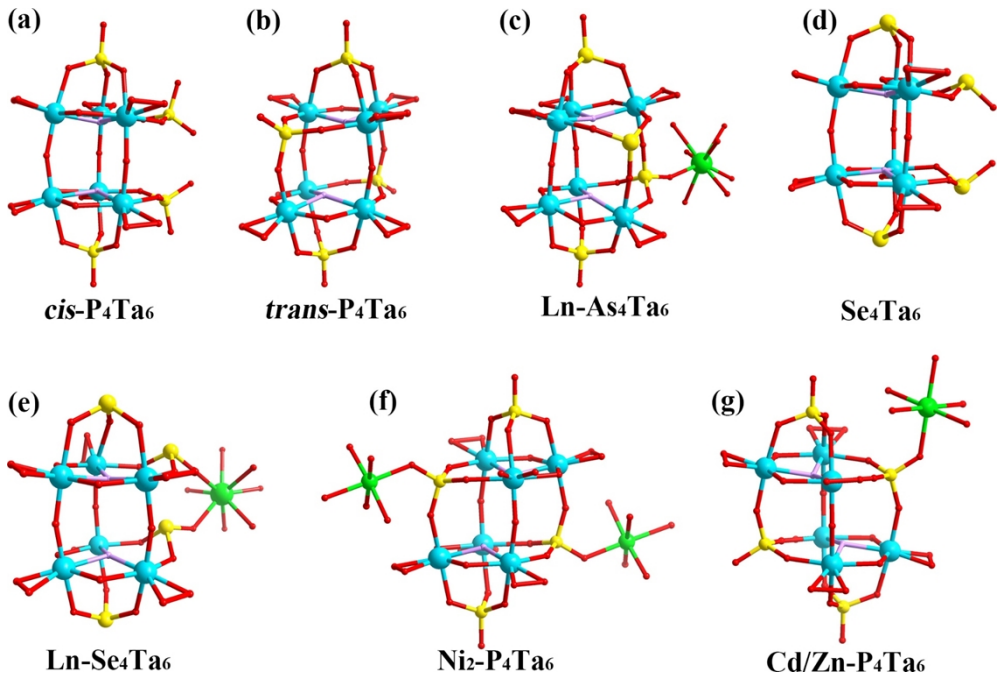

Fig. S3. The ball-and-stick representations of {*cis*-P_4Ta_6} (a), {*trans*-P_4Ta_6} (b), {Ln-As_4Ta_6} (c), {Se_4Ta_6} (d), {Ln-Se_4Ta_6} (e), {Ni_2-P_4Ta_6} (f), {Cd-P_4Ta_6} and {Zn-P_4Ta_6} (g). Color code: sea blue spheres: Ta; lavender spheres: μ_3-O spheres; red spheres: O; yellow spheres: P, As, Se; green spheres: Ln, Ni, Cd, and Zn.

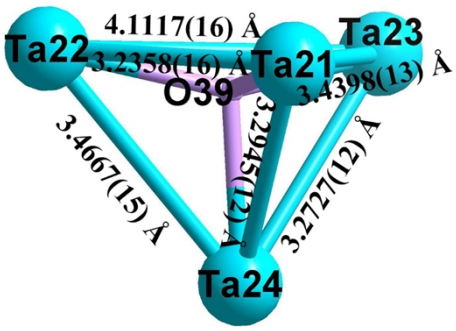

Fig. S4. The isosceles tetrahedron consists of Ta atoms in different positions. (∠Ta23Ta22Ta24=50.292°, ∠Ta21Ta22Ta24=58.762°, ∠Ta23Ta22Ta21=54.256°, ∠Ta22Ta24Ta23=75.130°, ∠Ta21Ta24Ta23=63.172°, ∠Ta22Ta24Ta21=57.118°, ∠Ta22Ta21Ta24=64.120°, ∠Ta23Ta21Ta24=58.106°, ∠Ta22Ta21Ta23=75.969°, ∠Ta22Ta23Ta21=49.774°, ∠Ta21Ta23Ta24=58.723°, ∠Ta22Ta23Ta24=54.578°.)

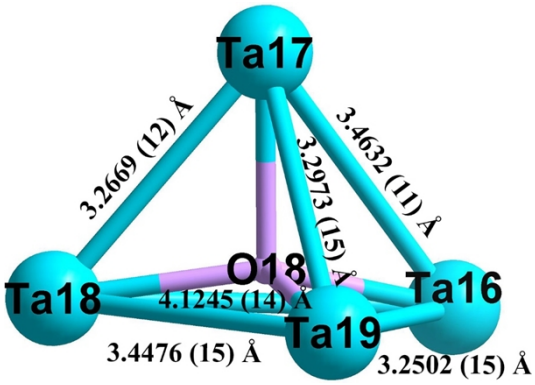

Fig. S5. The isosceles tetrahedron consists of Ta atoms in different positions. (∠Ta17Ta18Ta16=54.391°, ∠Ta17Ta18Ta19=58.749°, ∠Ta16Ta18Ta19=49.859°,∠Ta18Ta17Ta16=75.528°, ∠Ta18Ta17Ta19=63.362°, ∠Ta16Ta17Ta19=57.407°,∠Ta18Ta16Ta19=54.183°, ∠Ta17Ta16Ta19=58.732°, ∠Ta18Ta16Ta19=54.183°,∠Ta18Ta19Ta16=75.957°, ∠Ta18Ta19Ta17=57.889°, ∠Ta17Ta19Ta16=63.863°.)

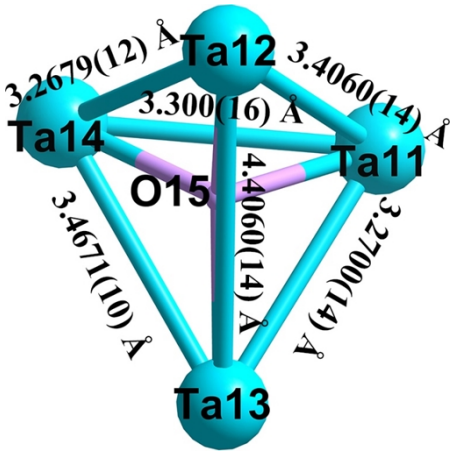

Fig. S6. The isosceles tetrahedron consists of Ta atoms in different positions. (∠Ta12Ta14Ta11=62.472°, ∠Ta12Ta14Ta13=74.885°, ∠Ta11Ta14Ta13=57.727°,∠Ta14Ta12Ta11=59.226°, ∠Ta14Ta12Ta13=54.770°, ∠Ta11Ta12Ta13=50.648°,∠Ta12Ta11Ta14=58.302°, ∠Ta14Ta11Ta13=63.702°, ∠Ta12Ta11Ta13=75.700°,∠Ta14Ta13Ta11=58.570°, ∠Ta12Ta13Ta11=53.652°, ∠Ta14Ta13Ta12=50.345°.)

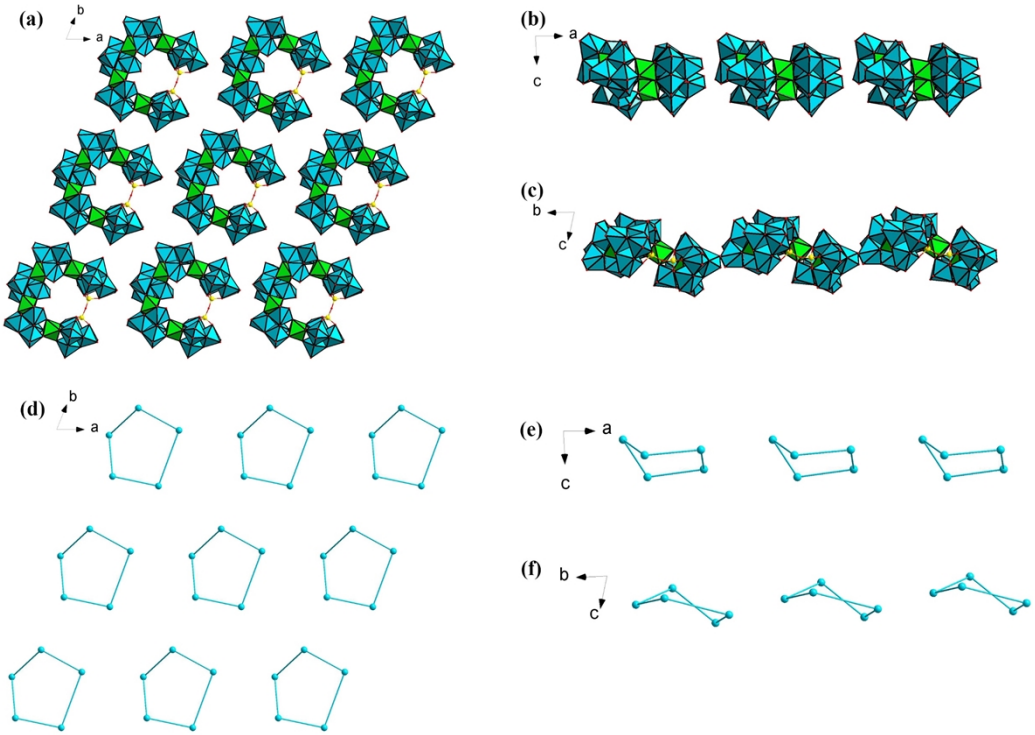

Fig. S7. The packing arrangements of polyoxoanion **1a** along the *a*(a), *b*(b) and *c*(c)-axis, respectively. And simplified 2D packing scheme for **1a** along the *a*(d), *b*(e) and *c*(f)-axis, respectively.

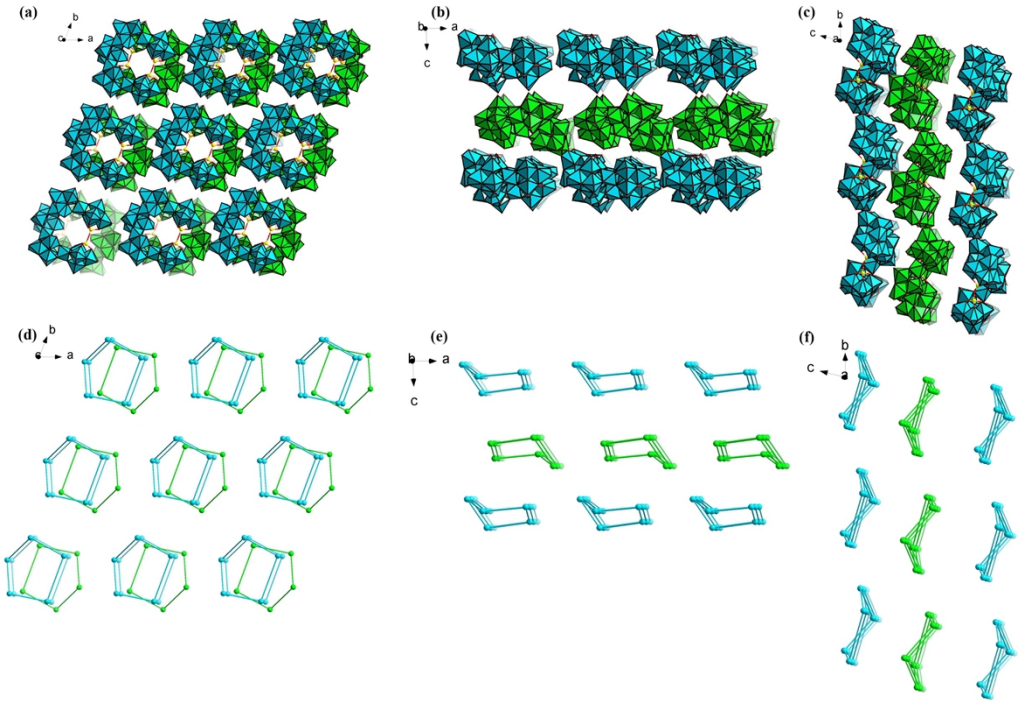

Fig. S8. Polyhedral views of the 3D stacking for **1a** along the *a*(a), *b*(b) and *c*(c)-axis, respectively. And simplified 3D packing scheme for **1a** along the *a*(d), *b*(e) and *c*(f)-axis, respectively.

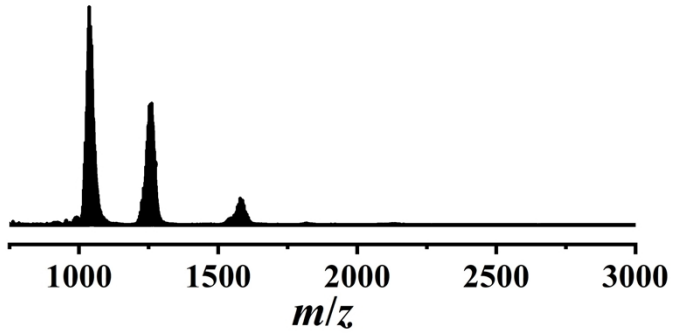

Fig. S9. ESI-MS spectra corresponding to the intact cluster of **1**.

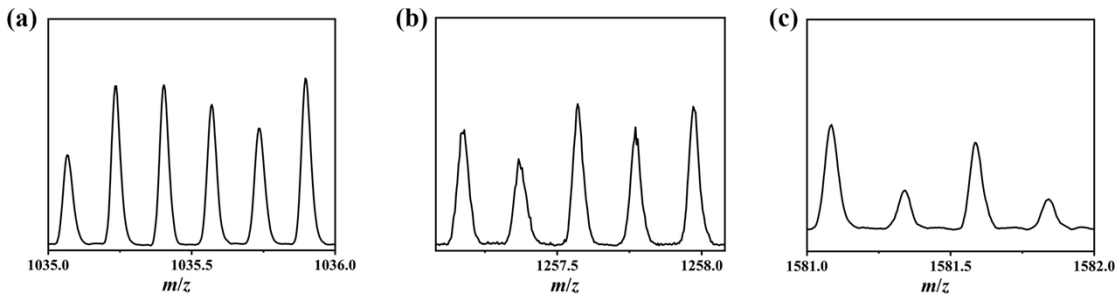

Fig. S10. Expanded region of the group of signals observed in the negative ESI mass spectrum of **1** illustrating the 6– charge state in a), 5– in b) and 4– in c).

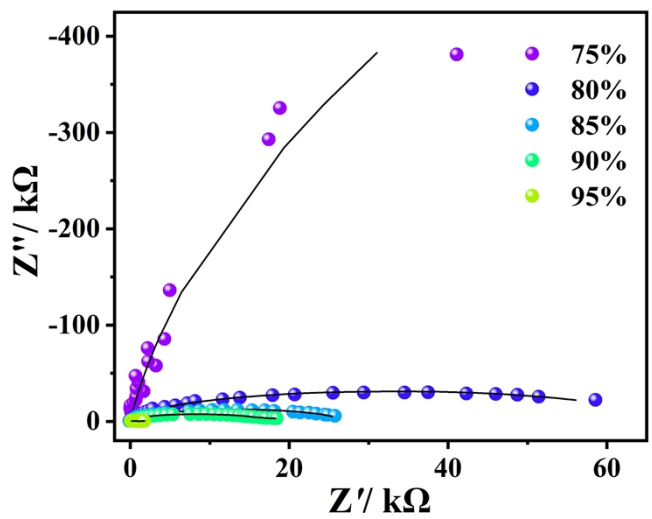

Fig. S11. Nyquist plots for **1** under different RHs at 25 °C. The solid lines are the best fits.

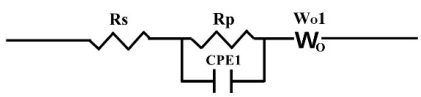

Fig. S12. The equivalent circuit is used for fitting.

In the electrical equivalent circuit (see above), Rs is the ohmic resistance of the bulk/grain, Rp is

the charge transfer resistance at the grain boundary/electrode interface (two identical charge transfer resistances connected in series) and CPE1 is a constant phase element used for imperfect capacitors, Wo1 is inductance representing the effect of the external circuit.

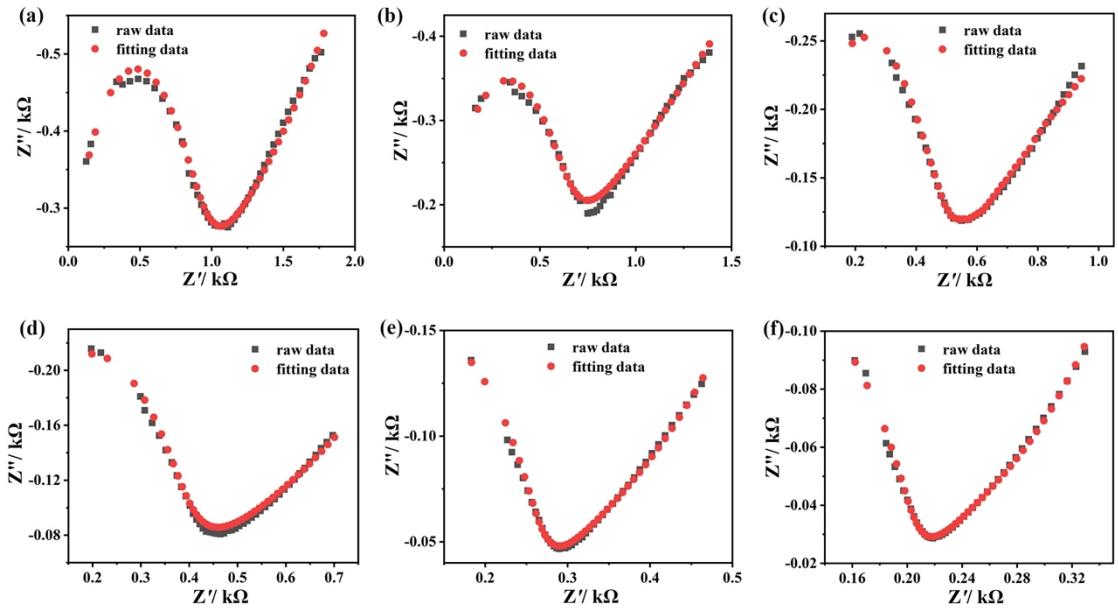

Fig. S13. Fitted data of **1** under different temperatures at 95% RH. (a): 25°C; (b): 35°C, (c): 45°C; (d): 55°C; (e):65°C, and (f): 75°C.

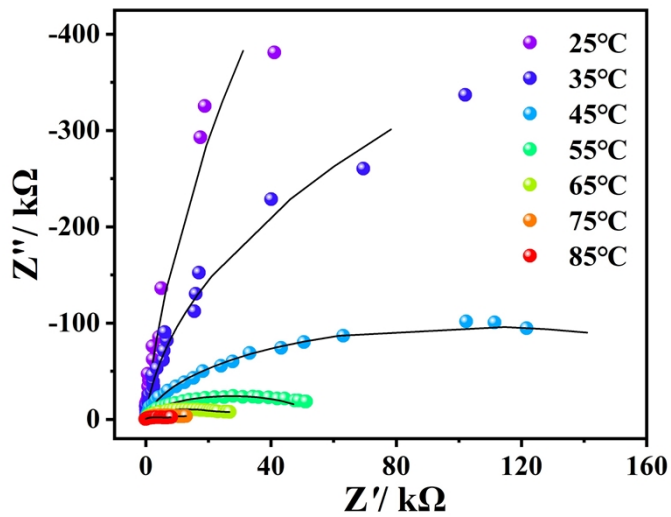

Fig. S14. Nyquist plots for **1** under different temperatures at 75% RH. The solid lines are the best fits.

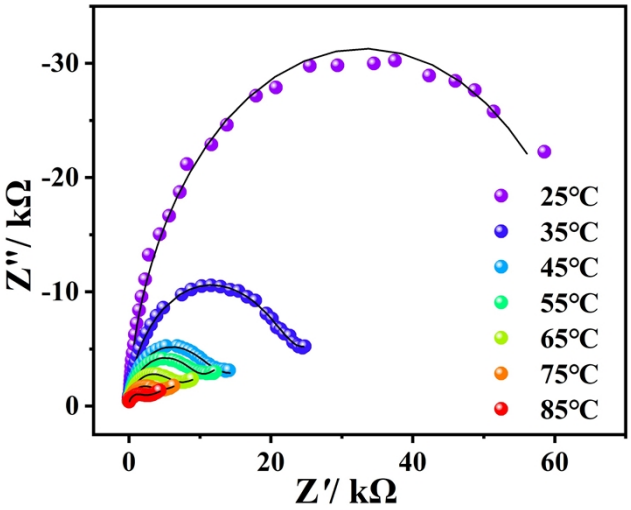

Fig. S15. Nyquist plots for **1** under different temperatures at 80% RH. The solid lines are the best fits.

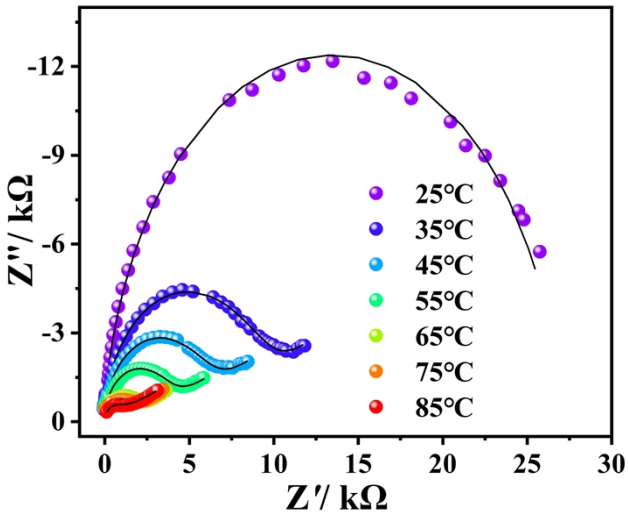

Fig. S16. Nyquist plots for **1** under different temperatures at 85% RH. The solid lines are the best fits.

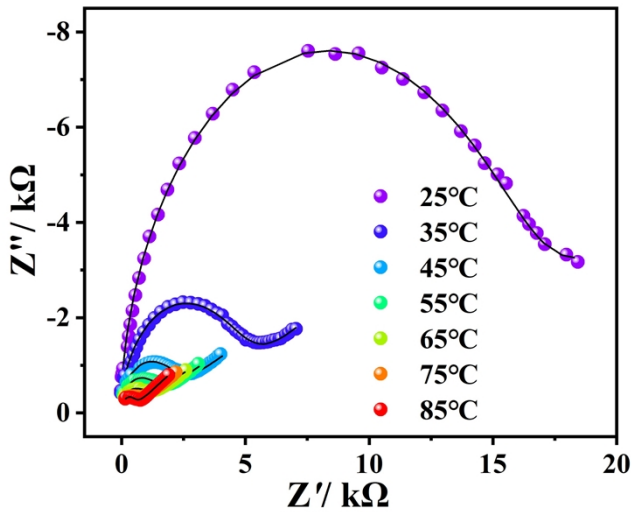

Fig. S17. Nyquist plots for **1** under different temperatures at 90% RH. The solid lines are the best fits.

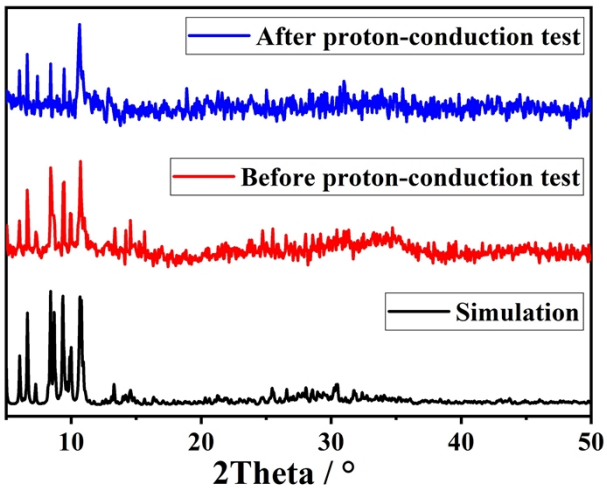

Fig. S18. PXRD of **1** calculated (black), crystalline sample (red), and after the proton-conductive measurement (blue).

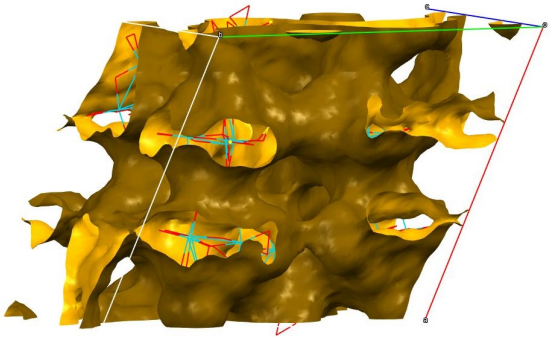

Fig. S19. Void analysis of **1**.

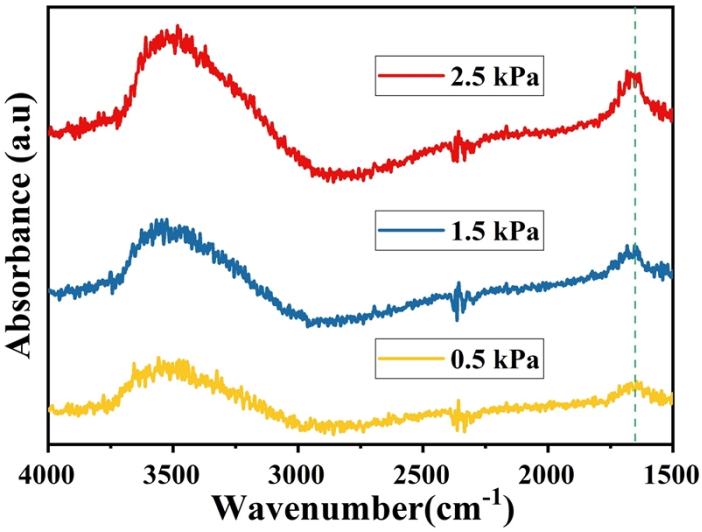

Fig. S20. In situ IR spectra of **1** under different water vapor pressure.

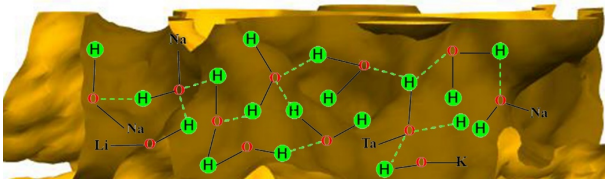

Fig. S21. Schematic diagram of hydrogen bonding networks consisting of water molecules inside the pore channels.

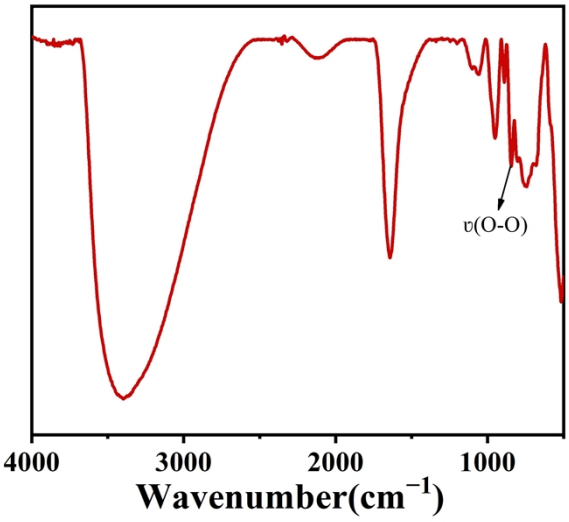

Fig. S22. IR spectrum of **1**.

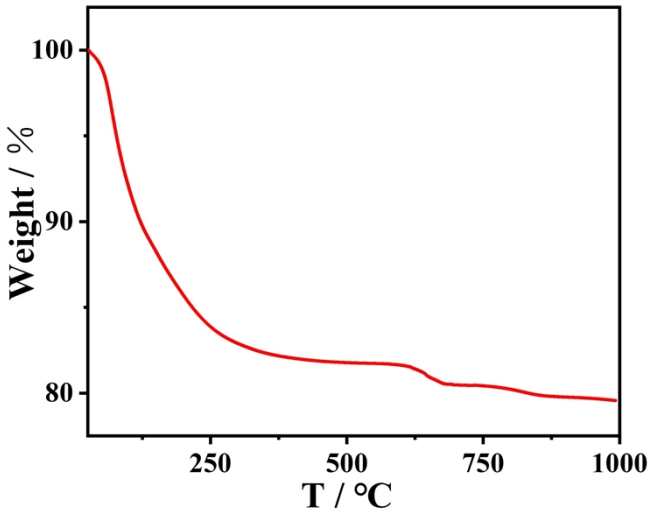

Fig. S23. TG curve of **1**.

References

1 M. Filowitz, R. K. C. Ho, W. G. Klemperer and W. Shum, Oxygen-17 nuclear magnetic resonance spectroscopy of polyoxometalates. 1. Sensitivity and resolution, *Inorg. Chem.*, 1979, **18**, 93–103.

2 Gilbert. Herve and Andre. Teze, Study of .alpha.- and .beta.-enneatungstosilicates and -germanates, *Inorg. Chem.*, 1977, **16**, 2115–2117.

3 G. M. Sheldrick, Crystal structure refinement with SHELXL, *Acta Crystallogr. Sect. C Struct. Chem.*, 2015, **71**, 3–8.

4 M. Nyman, F. Bonhomme, T. M. Alam, M. A. Rodriguez, B. R. Cherry, J. L. Krumhansl, T. M. Nenoff and A. M. Sattler, A General Synthetic Procedure for Heteropolyniobates, *Science*, 2002, **297**, 996–998.

5 M. Nyman, F. Bonhomme, T. M. Alam, J. B. Parise and G. M. B. Vaughan, $[SiNb_{12}O_{40}]^{16-}$ and $[GeNb_{12}O_{40}]^{16-}$: Highly Charged Keggin Ions with Sticky Surfaces, *Angew. Chem. Int. Ed.*, 2004, **43**, 2787–2792.

6 F. Bonhomme, J. P. Larentzos, T. M. Alam, E. J. Maginn and M. Nyman, Synthesis, Structural Characterization, and Molecular Modeling of Dodecaniobate Keggin Chain Materials, *Inorg. Chem.*, 2005, **44**, 1774–1785.

7 M. Nyman, A. J. Celestian, J. B. Parise, G. P. Holland and T. M. Alam, Solid-State Structural Characterization of a Rigid Framework of Lacunary Heteropolyniobates, *Inorg. Chem.*, 2006, **45**, 1043–1052.

8 T. M. Anderson, S. G. Thoma, F. Bonhomme, M. A. Rodriguez, H. Park, J. B. Parise, T. M. Alam, J. P. Larentzos and M. Nyman, Lithium Polyniobates. A Lindqvist-Supported Lithium-Water Adamantane Cluster and Conversion of Hexaniobate to a Discrete Keggin Complex, *Cryst. Growth Des.*, 2007, **7**, 719–723.

9 M. Nyman, J. P. Larentzos, E. J. Maginn, M. E. Welk, D. Ingersoll, H. Park, J. B. Parise, I. Bull and F. Bonhomme, Experimental and Theoretical Methods to Investigate Extraframework Species in a Layered Material of Dodecaniobate Anions, *Inorg. Chem.*, 2007, **46**, 2067–2079.

10 Z. Zhang, Q. Lin, D. Kurunthu, T. Wu, F. Zuo, S.-T. Zheng, C. J. Bardeen, X. Bu and P. Feng, Synthesis and Photocatalytic Properties of a New Heteropolyoxoniobate Compound: $K_{10}[Nb_2O_2(H_2O)_2][SiNb_{12}O_{40}]\cdot 12H_2O$, *J. Am. Chem. Soc.*, 2011, **133**, 6934–6937.

11 Y. Hou, M. Nyman and M. A. Rodriguez, Soluble Heteropolyniobates from the Bottom of Group IA, *Angew. Chem. Int. Ed.*, 2011, **50**, 12514–12517.

12 G. Guo, Y. Xu, J. Cao and C. Hu, An unprecedented vanadoniobate cluster with 'trans-vanadium' bicapped Keggin-type $\{VNb_{12}O_{40}(VO)_2\}$, *Chem. Commun.*, 2011, **47**, 9411–9413.

13 P. Huang, C. Qin, X.-L. Wang, C.-Y. Sun, G.-S. Yang, K.-Z. Shao, Y.-Q. Jiao, K. Zhou and Z.-M. Su, An unprecedented organic-inorganic hybrid based on the first $\{Nb_{10}V_4O_{40}(OH)_2\}^{12-}$ clusters and copper cations, *Chem. Commun.*, 2012, **48**, 103–105.

14 Y. Hou, T. M. Alam, M. A. Rodriguez and M. Nyman, Aqueous compatibility of group IIIA monomers and Nb-polyoxoanions, *Chem. Commun.*, 2012, **48**, 6004–6006.

15 G. Guo, Y. Xu, J. Cao and C. Hu, The $\{V_4Nb_6O_{30}\}$ Cluster: A New Type of Vanadoniobate Anion Structure, *Chem. - Eur. J.*, 2012, **18**, 3493–3497.

16 P. Huang, C. Qin, X.-L. Wang, C.-Y. Sun, Y. Xing, H.-N. Wang, K.-Z. Shao and Z.-M. Su, A new organic-inorganic hybrid based on the crescent-shaped polyoxoanion $[H_6SiNb_{18}O_{54}]^{8-}$ and copper-organic cations, *Dalton Trans.*, 2012, **41**, 6075–6077.

17 J.-H. Son, C. A. Ohlin, R. L. Johnson, P. Yu and W. H. Casey, A Soluble Phosphorus-Centered Keggin Polyoxoniobate with Bicapping Vanadyl Groups, *Chem. - Eur. J.*, 2013, **19**, 5191–5197.

18 J.-Q. Shen, S. Yao, Z.-M. Zhang, H.-H. Wu, T.-Z. Zhang and E.-B. Wang, Self-assembly and photocatalytic property of germanoniobate $[H_6Ge_4Nb_{16}O_{56}]^{10-}$: encapsulating four $\{GeO_4\}$ tetrahedra within a $\{Nb_{16}\}$ cage, *Dalton Trans.*, 2013, **42**, 5812–5817.

19 X. Zhang, S. Liu, S. Li, Y. Gao, X. Wang, Q. Tang and Y. Liu, Two Members of the $\{X_4Nb_{16}O_{56}\}$ Family (X = Ge, Si) Based on $[(GeOH)_2Ge_2Nb_{16}H_2O_{54}]^{12-}$ and $[K(GeOH)_2Ge_2Nb_{16}H_3O_{54}]^{10-}$, *Eur. J. Inorg. Chem.*, 2013, **2013**, 1706–1712.

20 J. Son, C. A. Ohlin, E. C. Larson, P. Yu and W. H. Casey, Synthesis and Characterization of a Soluble Vanadium-Containing Keggin Polyoxoniobate by ESI-MS and ^{51}V NMR: $(TMA)_9[V_3Nb_{12}O_{42}]\cdot 18H_2O$, *Eur. J. Inorg. Chem.*, 2013, **2013**, 1748–1753.

21 Y. Hou, L. N. Zakharov and M. Nyman, Observing Assembly of Complex Inorganic Materials from Polyoxometalate Building Blocks, *J. Am. Chem. Soc.*, 2013, **135**, 16651–16657.

22 J.-H. Son, J. Wang, F. E. Osterloh, P. Yu and W. H. Casey, A tellurium-substituted Lindqvist-type polyoxoniobate showing high H_2 evolution catalyzed by tellurium nanowires *via* photodecomposition, *Chem. Commun.*, 2014, **50**, 836–838.

23 J.-Q. Shen, Y. Zhang, Z.-M. Zhang, Y.-G. Li, Y.-Q. Gao and E.-B. Wang, Polyoxoniobate-based 3D framework materials with photocatalytic hydrogen evolution activity, *Chem. Commun.*, 2014, **50**, 6017–6019.

24 J. Shen, Q. Wu, Y. Zhang, Z. Zhang, Y. Li, Y. Lu and E. Wang, Unprecedented High-Nuclear Transition-Metal-Cluster-Substituted Heteropolyoxoniobates: Synthesis by $\{V_8\}$ Ring Insertion into the POM Matrix and Antitumor Activities, *Chem. - Eur. J.*, 2014, **20**, 2840–2848.

25 Y. Zhang, J.-Q. Shen, L.-H. Zheng, Z.-M. Zhang, Y.-X. Li and E.-B. Wang, Four Polyoxonibate-Based Inorganic-Organic Hybrids Assembly from Bicapped Heteropolyoxonibate with Effective Antitumor Activity, *Cryst. Growth Des.*, 2014, **14**, 110–116.

26 J.-H. Son and W. H. Casey, Reversible capping/uncapping of phosphorous-centered Keggin-type polyoxoniobate clusters, *Chem. Commun.*, 2015, **51**, 1436–1438.

27 J.-H. Son and W. H. Casey, A new Keggin-like niobium-phosphate cluster that reacts reversibly with hydrogen peroxide, *Chem. Commun.*, 2015, **51**, 12744–12747.

28 Q. Lan, Z.-M. Zhang, Y.-G. Li and E.-B. Wang, Extended structural materials composed of transition-metal-substituted arsenicniobates and their photocatalytic activity, *RSC Adv.*, 2015, **5**, 44198–44203.

29 J.-F. Hu, T. Han, Y.-N. Chi, Z.-G. Lin, Y.-Q. Xu, S. Yang, D. Wei, Y.-Z. Zheng and C.-W. Hu, Sulfur-centred polyoxoniobate-based 3D organic-inorganic hybrid compound and its magnetic behavior, *Chem. Commun.*, 2016, **52**, 10846–10849.

30 P. A. Abramov, A. T. Davletgildeeva, N. K. Moroz, N. B. Kompankov, B. Santiago-Schübel and M. N. Sokolov, Cation-Dependent Self-assembly of Vanadium Polyoxoniobates, *Inorg. Chem.*, 2016, **55**, 12807–12814.

31 N. Li, Y. Liu, Y. Lu, D. He, S. Liu, X. Wang, Y. Li and S. Liu, An arsenicniobate-based 3D framework with selective adsorption and anion-exchange properties, *New J. Chem.*, 2016, **40**, 2220–2224.

32 J. Dong, J. Hu, Y. Chi, Z. Lin, B. Zou, S. Yang, C. L. Hill and C. Hu, A Polyoxoniobate-Polyoxovanadate Double-Anion Catalyst for Simultaneous Oxidative and Hydrolytic Decontamination of Chemical Warfare Agent Simulants, *Angew. Chem. Int. Ed.*, 2017, **56**, 4473–4477.

33 L. Jin, Z. Zhu, Y. Wu, Y. Qi, X. Li and S. Zheng, Record High-Nuclearity Polyoxoniobates: Discrete Nanoclusters $\{Nb_{114}\}$, $\{Nb_{81}\}$, and $\{Nb_{52}\}$, and Extended Frameworks Based on $\{Cu_3Nb_{78}\}$ and $\{Cu_4Nb_{78}\}$, *Angew. Chem. Int. Ed.*, 2017, **56**, 16288–16292.

34 L. Li, K. Dong, P. Ma, C. Zhang, J. Niu and J. Wang, An $\{As_4Cu_4[Cu(H_2O)]_{12}\}$ Cluster Incorporated within Four $[Nb_7O_{22}]^{9-}$ Units, *Chem. - Eur. J.*, 2017, **23**, 16957–16960.

35 Z. Liang, K. Wang, D. Zhang, P. Ma, J. Niu and J. Wang, $\{Fe_3Nb_{25}\}$ cluster based on an Fe-centred Keggin unit, *Dalton Trans.*, 2017, **46**, 1368–1371.

36 J. Hu, J. Dong, X. Huang, Y. Chi, Z. Lin, J. Li, S. Yang, H. Ma and C. Hu, Immobilization of Keggin polyoxovanadoniobate in crystalline solids to produce effective heterogeneous catalysts towards selective oxidation of benzyl-alkanes, *Dalton Trans.*, 2017, **46**, 8245–8251.

37 Z. Liang, J. Sun, D. Zhang, P. Ma, C. Zhang, J. Niu and J. Wang, Assembly of TeO_3^{2-} Ions Embedded in an Nb/O Cage with Selective Decolorization of Organic Dye, *Inorg. Chem.*, 2017, **56**, 10119–10122.

38 B.-X. Liu, Z.-W. Cai, T. Yang, X.-X. Li, G.-Y. Yang and S.-T. Zheng, A rare polyoxometalate based on mixed niobium-based polyoxoanions $[GeNb_{18}O_{54}]^{14-}$ and $[Nb_3W_3O_{19}]^{5-}$, *Inorg. Chem. Commun.*, 2017, **78**, 56–60.

39 T.-T. Zhang, X. Zhang, Y. Lü, G.-D. Li, L.-N. Xiao, X.-B. Cui and J.-Q. Xu, New organic-inorganic hybrid compounds based on $[SiNb_{12}V_2O_{42}]^{12-}$ with high catalytic activity for styrene epoxidation, *Inorg. Chem. Front.*, 2017, **4**, 1397–1404.

40 Z. Liang, L. Zhang, Y. Li, P. Ma, J. Niu and J. Wang, Two Novel Heteropolyniobates Using TeO_3^{2-} as Template and Linker, *Inorg. Chem.*, 2019, **58**, 27–30.

41 Y.-Y. Lin, J. Zhang, Z.-K. Zhu, Y.-Q. Sun, X.-X. Li and S.-T. Zheng, An ultrastable {SiNb18O54}-based hybrid polyoxoniobate framework for selective removal of crystal violet from aqueous solution and proton-conduction, *Inorg. Chem. Commun.*, 2020, **113**, 107766.

42 T.-T. Zhang, P.-H. Lin, G.-Y. Yu, X. Zhang and X.-B. Cui, Syntheses, characterization and properties of two new dodeca-niobates presenting unprecedented features, *Dalton Trans.*, 2020, **49**, 6495–6503.

43 Z. Liang, Y. He, Y. Qiao, P. Ma, J. Niu and J. Wang, Sandwich-Type Heteropolyniobate Templated by Mixed Heteroanions, *Inorg. Chem.*, 2020, **59**, 7895–7899.

44 Y.-L. Wu, Y.-Q. Sun, X.-X. Li and S.-T. Zheng, A new dimeric isopolyoxoniobate {β-$H_4Nb_{52}O_{150}$} decorated with copper(II)-ethylenediamine for hydrolytic decomposition of chemical warfare agent simulant DMMP, *Inorg. Chem. Commun.*, 2020, **113**, 107815.

45 Z. Liang, J. Yu, Y. Zhang, P. Ma, Q. Mao and J. Wang, A lacunary heteropolyniobate linked by $[Co(H_2O)_6]^{2+}$ ions, *Inorg. Chem. Commun.*, 2020, **111**, 107612.

46 Z. Yang, J. Shang, Y. He, Y. Qiao, P. Ma, J. Niu and J. Wang, A 1D Helical Chain Heterpolyniobate Templated by AsO_3^{3-}, *Inorg. Chem.*, 2020, **59**, 1967–1972.

47 Z. Liang, Y. Qiao, X. Li, P. Ma, J. Niu and J. Wang, A large copper-niobate cluster with the pagoda-shaped subunit {$Nb_{20}O_{59}$}, *Chem. Commun.*, 2021, **57**, 3999–4002.

48 Z. Yang, J. Shang, Y. Yang, P. Ma, J. Niu and J. Wang, Synthesis, structures and stability of three V-substituted polyoxoniobate clusters based on $[TeNb_9O_{33}]^{17-}$ units, *Dalton Trans.*, 2021, **50**, 7610–7620.

49 Y. Wu, Z. Zhong, P. Wu, Y. Sun, X. Li and S. Zheng, A Peanut-Like Sb-Embedded Polyoxoniobate Cage for Hydrolytic Decomposition of Chemical Warfare Agent, *Eur. J. Inorg. Chem.*, 2021, **2021**, 1505–1509.

50 P.-X. Wu, R.-D. Lai, R. Ge, C. Sun, G.-Q. Wang, X.-X. Li and S.-T. Zheng, A Tellurium-Substituted Heteropolyniobate with Unique π–π Stacking and Ionic Conduction Property, *Inorg. Chem.*, 2021, **60**, 6162–6166.

51 N. Shi, Y.-J. Wang, X.-X. Li, Y.-Q. Sun and S.-T. Zheng, An inorganic Co-containing heteropolyoxoniobate: reversible chemochromism and H_2O-dependent proton conductivity properties, *Inorg. Chem. Front.*, 2021, **8**, 5225–5233.

52 Z.-H. Zhong, J.-X. Jing, Y.-Q. Sun, X.-X. Li and S.-T. Zheng, Two new 3D tubular

polyoxoniobates frameworks based on $\{SiNb_{18}O_{54}\}$ clusters with proton conduction properties, *Inorg. Chem. Commun.*, 2021, **132**, 108813.

53 R.-D. Lai, H.-L. Feng, Y.-Q. Sun, X.-X. Li and S.-T. Zheng, A lanthanide-tellurium heterometal encapsulated sandwich-type heteropolyoxoniobate with a 3D pcu-type hydrogen-bonded network, *Dalton Trans.*, 2022, **51**, 10571–10577.

54 J. Son and W. H. Casey, Titanium-Substituted Polyoxotantalate Clusters Exhibiting Wide pH Stabilities: $[Ti_2Ta_8O_{28}]^{8-}$ and $[Ti_{12}Ta_6O_{44}]^{10-}$, *Chem. - Eur. J.*, 2016, **22**, 14155–14157.

55 D. Zhang, Z. Liang, S. Liu, L. Li, P. Ma, S. Zhao, H. Wang, J. Wang and J. Niu, Discovery of Heteropolytantalate: Synthesis and Structure of Two 6-Peroxotantalo-4-phosphate Clusters, *Inorg. Chem.*, 2017, **56**, 5537–5543.

56 Z. Liang, H. Wu, V. Singh, Y. Qiao, M. Li, P. Ma, J. Niu and J. Wang, Assembly of Lanthanide-Containing Polyoxotantalate Clusters with Efficient Photoluminescence Properties, *Inorg. Chem.*, 2019, **58**, 13030–13036.

57 H. Wang, J. Sun, Y. Ma, C. Li, N. Li, P. Ma, D. Zhang, G. Wang, J. Wang and J. Niu, Discovery of the selenotantalate building block and its lanthanide derivatives: design, synthesis, and RhB decolorization properties, *Dalton Trans.*, 2020, **49**, 4078–4083.

58 X. Li, H. Zhao, Y. Li, Y. Yang, M. Zhang, S. Liu, P. Ma, J. Wang and J. Niu, Synthesis, structure and properties of three novel transition-metal-containing tantalum-phosphate clusters, *Chin. Chem. Lett.*, 2022, **33**, 4675–4678.

59 Y. Guan, H.-B. Chen, R. Ge, Q.-X. Zeng, P.-W. Cai, C. Sun, Y.-Q. Sun, X.-X. Li and S.-T. Zheng, Development of a New Heteropolyoxotantalate Cluster for Multidimensional Polyoxotantalate Materials, *Inorg. Chem.*, 2023, **62**, 10044–10048.

60 D. A. Judd, Q. Chen, C. F. Campana and C. L. Hill, Synthesis, Solution and Solid State Structures, and Aqueous Chemistry of an Unstable Polyperoxo Polyoxometalate: $[P_2W_{12}(NbO_2)_6O_{56}]^{12-}$, *J. Am. Chem. Soc.*, 1997, **119**, 5461–5462.

61 S.-J. Li, S.-X. Liu, C.-C. Li, F.-J. Ma, D.-D. Liang, W. Zhang, R.-K. Tan, Y.-Y. Zhang and L. Xu, Reactivity of Polyoxoniobates in Acidic Solution: Controllable Assembly and Disassembly Based on Niobium-Substituted Germanotungstates, *Chem. - Eur. J.*, 2010, **16**, 13435–13442.

62 S.-J. Li, S.-X. Liu, C.-C. Li, F.-J. Ma, W. Zhang, D.-D. Liang, R.-K. Tan, Y.-Y. Zhang and Q. Tang, Niobium-substituted arsenotungstates: Controllable transformation between monomers and tetramer, *Inorg. Chim. Acta.*, 2011, **376**, 296–301.

63 M. Carraro, N. Nsouli, H. Oelrich, A. Sartorel, A. Sorarù, S. S. Mal, G. Scorrano, L. Walder, U. Kortz and M. Bonchio, Reactive Zr^{IV} and Hf^{IV} Butterfly Peroxides on Polyoxometalate Surfaces: Bridging the Gap between Homogeneous and Heterogeneous Catalysis, *Chem. - Eur. J.*, 2011, **17**, 8371–8378.

64 P. Miró, J. Ling, J. Qiu, P. C. Burns, L. Gagliardi and C. J. Cramer, Experimental and Computational Study of a New Wheel-Shaped $\{[W_5O_{21}]_3[(U^{VI}O_2)_2(\mu\text{-}O_2)]_3\}^{30-}$ Polyoxometalate, *Inorg. Chem.*, 2012, **51**, 8784–8790.

65 S. Li, S. Liu, S. Liu, Y. Liu, Q. Tang, Z. Shi, S. Ouyang and J. Ye, $\{Ta_{12}\}/\{Ta_{16}\}$ Cluster-Containing Polytantalotungstates with Remarkable Photocatalytic H_2 Evolution Activity, *J. Am. Chem. Soc.*, 2012, **134**, 19716–19721.

66 Y. Ren, Y. Hu, Y. Shan, Z. Kong, M. Gu, B. Yue and H. He, A mixed-addenda Nb/W polyoxometalate containing dimeric Dawson subunit: Synthesis, structure, and characterization, *Inorg. Chem. Commun.*, 2014, **40**, 108–111.

67 H. M. Qasim, W. W. Ayass, P. Donfack, A. S. Mougharbel, S. Bhattacharya, T. Nisar, T. Balster, A. Solé-Daura, I. Römer, J. Goura, A. Materny, V. Wagner, J. M. Poblet, B. S. Bassil and U. Kortz, Peroxo-Cerium(IV)-Containing Polyoxometalates: $[Ce^{IV}_6(O_2)_9(GeW_{10}O_{37})_3]^{24-}$, a Recyclable Homogeneous Oxidation Catalyst, *Inorg. Chem.*, 2019, **58**, 11300–11307.

68 W. Du, Y. Liu, J. Sun, H. Wang, G. Yang and D. Zhang, Three rare-earth incorporating 6-peroxotantalo-4-selenates and catalytic activities for imidation reaction, *Dalton Trans.*, 2022, **51**, 9988–9993.

69 H. Chen, M. Zhang, Y. Li, P. Ma, J. Wang and J. Niu, *Chem. Commun.*, 2023, **59**, 10664–10667.

70 Y. Yu, R.-D. Lai, C. Sun, Y.-Q. Sun, Q.-X. Zeng, X.-X. Li and S.-T. Zheng, Oxalate-assisted assembly of two polyoxotantalate supramolecular frameworks with proton conduction properties, *Chem. Commun.*, 2023, **59**, 3735–3738.

71 Z. Li, J. Zhang, L.-D. Lin, J.-H. Liu, X.-X. Li and S.-T. Zheng, Inorganic-organic hybrid high-dimensional polyoxotantalates and their structural transformations triggered by water, *Chem. Commun.*, 2019, **55**, 11735–11738.

72 Y.-L. Wang, Y.-L. Wu, Q.-X. Zeng, X.-X. Li and S.-T. Zheng, Two new inorganic-organic hybrid polyoxotantalates with proton conduction property, *J. Solid State Chem.*, 2023, **322**, 123943.

73 Y.-J. Wang, L. Yu, X.-X. Li, Y.-Q. Sun and S.-T. Zheng, Two Unprecedented Germanoniobate Frameworks Based on High-Nuclearity Peanut-Shaped $\{Ge_{12}Nb_{38}\}$ Clusters, *Inorg. Chem.*, 2024, **63**, 1388–1394.

74 Y. Sun, H. Li, Y. Zou, P. Ma, J. Niu and J. Wang, A Hexameric Ruthenium(III)-Containing Tungstoantimonate with Good Proton Conductivity Performance, *Inorg. Chem.*, 2023, **62**, 14142–14146.

75 M. Yang, H. Li, Y. Zhang, S. Ji, W. Chen, P. Ma, J. Wang and J. Niu, Organic Hybrid Antimoniotungstate Layered Ionic Crystal: Synthesis, Structure, and Interlayer-Confined Proton Conduction, *Inorg. Chem.*, 2023, **62**, 6467–6473.

76 R.-D. Lai, J. Zhang, X.-X. Li, S.-T. Zheng and G.-Y. Yang, Assemblies of Increasingly Large Ln-Containing Polyoxoniobates and Intermolecular Aggregation-Disaggregation Interconversions, *J. Am. Chem. Soc.*, 2022, **144**, 19603–19610.

77 K. Zheng, D. Yang, B. Niu, Y. Ye, P. Ma, J. Wang and J. Niu, $_{DL}$-Alanine Covalently Bonded Giant Arsenotungstate with Rapid Photochromic and Decent Proton Conduction Properties, *Inorg. Chem.*, 2022, **61**, 20222–20226.

78 H. Chen, K. Zheng, J. Wang, B. Niu, P. Ma, J. Wang and J. Niu, Discovery and Isolation of Two Arsenotungastate Species: $[As_4W_{48}O_{168}]^{36-}$ and $[As_2W_{21}O_{77}(H_2O)_3]^{22-}$, *Inorg. Chem.*, 2023, **62**, 3338–3342.

79 R.-D. Lai, Z.-K. Zhu, Y. Wu, Y.-Q. Sun, C. Sun, X.-X. Li and S.-T. Zheng, Proton-Conductive Polyoxometalate Architectures Constructed from Lanthanide-Incorporated Polyoxoniobate Cages, *Inorg. Chem.*, 2022, **61**, 21047–21054.

80 Y.-H. Fan, M. Du, Y.-X. Li, W.-J. Zhu, J.-Y. Pang, Y. Bai and D.-B. Dang, Construction of Water-Stable Rare-Earth Organic Frameworks with Ambient High Proton Conductivity Based on Zirconium Sandwiched Heteropolytungstate, *Inorg. Chem.*, 2022, **61**, 13829–13835.

81 Z. Jing, W. Wang, R. Wan, X. Ma, Y. Qiao, Y. Bai, P. Ma, J. Niu and J. Wang, Rocket-Shaped Telluroniobate with Efficient Catalytic Activity in the Transesterification Reaction, *Inorg. Chem.*, 2022, **61**, 16528–16532.

82 Y.-D. Lin, Z.-K. Zhu, R. Ge, H. Yu, Z. Li, C. Sun, Y.-Q. Sun, X.-X. Li and S.-T. Zheng, Proton conductive polyoxoniobate frameworks constructed from nanoscale $\{Nb_{68}O_{200}\}$ cages, *Chem. Commun.*, 2021, **57**, 4702–4705.

83 C. Si, P. Ma, Q. Han, J. Jiao, W. Du, J. Wu, M. Li and J. Niu, A Polyoxometalate-Based Inorganic Porous Material with both Proton and Electron Conductivity by Light Actuation: Photocatalysis for Baeyer-Villiger Oxidation and Cr(VI) Reduction, *Inorg. Chem.*, 2021, **60**, 682–691.

84 S. Li, Y. Zhao, S. Knoll, R. Liu, G. Li, Q. Peng, P. Qiu, D. He, C. Streb and X. Chen, High Proton-Conductivity in Covalently Linked Polyoxometalate-Organoboronic Acid-Polymers, *Angew. Chem. Int. Ed.*, 2021, **60**, 16953–16957.

85 J. Liu, Q. Han, L. Chen, J. Zhao, C. Streb and Y. Song, Aggregation of Giant Cerium-Bismuth Tungstate Clusters into a 3D Porous Framework with High Proton Conductivity, *Angew. Chem. Int. Ed.*, 2018, **57**, 8416–8420.

86 P. Yang, M. Alsufyani, A. Emwas, C. Chen and N. M. Khashab, Lewis Acid Guests in a $\{P_8W_{48}\}$ Archetypal Polyoxotungstate Host: Enhanced Proton Conductivity via Metal-Oxo Cluster within Cluster Assemblies, *Angew. Chem. Int. Ed.*, 2018, **57**, 13046–13051.

87 Z. Li, L.-D. Lin, H. Yu, X.-X. Li and S.-T. Zheng, All-Inorganic Ionic Porous Material Based on Giant Spherical Polyoxometalates Containing Core-Shell $K_6@K_{36}$-Water Cage, *Angew. Chem. Int. Ed.*, 2018, **57**, 15777–15781.

88 Z. Li, X.-X. Li, T. Yang, Z.-W. Cai and S.-T. Zheng, Four-Shell Polyoxometalates Featuring High-Nuclearity Ln26 Clusters: Structural Transformations of Nanoclusters into Frameworks Triggered by Transition-Metal Ions, *Angew. Chem. Int. Ed.*, 2017, **56**, 2664–2669.

89 P. Ma, R. Wan, Y. Wang, F. Hu, D. Zhang, J. Niu and J. Wang, Coordination-Driven Self-Assembly of a 2D Graphite-Like Framework Constructed from High-Nuclear Ce_{10} Cluster Encapsulated Polyoxotungstates, *Inorg. Chem.*, 2016, **55**, 918–924.

90 Z. Liu, X. Zhang, R. Wan, H. Li, Y. Hong, P. Ma, J. Niu and J. Wang, A Rh-substituted polyoxometalate with an acetate-modified building block $\{As_2W_{22}O_{76}(CH_3COO)_2\}$, *Chem. Commun.*, 2021, **57**, 10250–10253.

91 E.-L. Zhou, C. Qin, P. Huang, X.-L. Wang, W.-C. Chen, K.-Z. Shao and Z.-M. Su, A Stable Polyoxometalate-Pillared Metal-Organic Framework for Proton-Conducting and Colorimetric Biosensing, *Chem. - Eur. J.*, 2015, **21**, 11894–11898.

92 Q. Peng, S. Li, R. Wang, S. Liu, L. Xie, J. Zhai, J. Zhang, Q. Zhao and X. Chen, Lanthanide derivatives of Ta/W mixed-addendum POMs as proton-conducting materials, *Dalton Trans.*, 2017, **46**, 4157–4160.

93 S. Chand, S. C. Pal, A. Pal, Y. Ye, Q. Lin, Z. Zhang, S. Xiang and M. C. Das, Metalo Hydrogen-Bonded Organic Frameworks (MHOFs) as New Class of Crystalline Materials for Protonic Conduction, *Chem. - Eur. J.*, 2019, **25**, 1691–1695.